Chapter 4

Morphology Development in Model Polyethylenes via Two-Dimensional Correlation Analysis

4.1 INTRODUCTION

The physical properties of semicrystalline polymeric materials are ultimately dictated by their morphology in the solid state. This morphology is a complex function of molecular characteristics (molecular weight, architecture, etc.), thermal history (cooling rate, etc.), and processing (shear stress, extensional flow rate, etc.). The large number of variables that affect the morphology, and hence material properties, has led to extensive studies that try to discern morphological development using techniques such as wide angle and small angle x-ray scattering (WAXS and SAXS, respectively).[1-15] Information relevant to the sample morphology is often discerned from many conventional x-ray data analysis techniques that involve the calculation of morphological parameters such as crystallinity (X_c), long period (L_p), and the SAXS integrated intensity (Q).

The application of such conventional techniques on SAXS and WAXS data obtained during crystallization of hydrogenated polybutadiene (HPBD) materials in Chapter 3 revealed that morphology development of these short-chain branched (SCB) materials during cooling can be separated into three crystallization regimes (Figure 3.15 in Chapter 3). 'Primary-irreversible' crystallization occurs at the highest temperatures and is marked by large changes in the morphological parameters (X_c, L_p, and Q) as primary lamellae propagate rapidly through unconstrained melt. Once the majority of unconstrained melt is consumed, secondary lamellar growth in the largest non-crystalline regions between primary lamellae marks slower 'secondary-irreversible' crystallization that occurs at intermediate temperatures. This temperature region is marked by slower changes in X_c and L_p and a nearly constant Q near its maximum value. The secondary-irreversible regime is not evident in homopolymers, such as HDPE, due to the relatively uniform and narrow

non-crystalline layer thickness in the primary lamellar stacks under the conditions examined. Both irreversible regimes obtain their names from the hysteresis that is observed between the morphological parameters during cooling and subsequent heating as a consequence of supercooling requirements for nucleation and growth of entangled polymers. At low temperatures, the values of the morphological parameters are equal during cooling and subsequent heating marking the slow formation of fringed micelles that occurs in the 'reversible' crystallization regime. Unlike homopolymers, reversible crystallization of random copolymers exhibits significant changes in X_c and L_p, which has important implications for physical aging of these materials.[16] Additionally, a decrease in Q observed when while X_c was below 50% is consistent with a decrease in electron density contrast during reversible crystallization of HPBDs. These three crystallization regimes exhibit unique and complex behavior, the understanding of which can aid in the control of material properties.

The complex evolution of morphology during crystallization of polymers can be better understood by examining x-ray scattering curves as a whole, rather than particular characteristics, such as peak location or area. Such an examination can be conducted using two-dimensional (2D) correlation analysis whose application is abundant in the field of vibrational spectroscopy.[17-20] This powerful technique allows for the examination of sometimes subtle changes in spectral intensities in response to a perturbation variable, such as temperature. This versatile analysis has been frequently applied to protein,[21-23] liquid crystal,[24, 25] and polymer[26-31] systems when studied by Raman or infrared spectroscopy. However, although the generalization of the 2D correlation analysis by Noda has allowed it to be easily applied to most three-dimensional datasets,[17-19] its application to

experimental data obtained using other probes, such as x-rays, has been surprisingly limited.[31, 32]

The application of 2D correlation analysis provides distinct advantages that can be utilized to extract information about morphology from x-ray scattering data during crystallization or melting. These advantages include the simplification of complex scattering curves through the de-convolution of overlapping features, the determination of sequential order of intensity changes, and the enhancement of spectral resolution by spreading data over a second dimension. Additionally, 2D moving window analysis (MW2D) allows for the examination of correlated intensity changes as a function of (versus a general response to) the perturbation variable.[17, 18, 31] Furthermore, heterospectral correlation analysis,[18] an extension of the conventional 2D method, allows one to directly visualize changes in SAXS and WAXS that are the result of the same physical processes.

This analysis can provide new insight into important aspects of polymer crystallization. For example, there has been significant debate behind the reasons for poor results when WAXS curves of ethylene copolymers are fitted for the purposes of crystallinity calculations using a two-phase model: one peak for the amorphous halo and one peak for each of the crystalline reflections.[4, 5, 7, 33-37] Some of these studies have noted that fitting the amorphous halo with two peaks yields a better fit and more reasonable behavior of all peaks considered (position, width, etc.).[4, 5, 7, 33, 34, 37] The physical justification of this additional peak is controversial. Observation of a hexagonal mesophase reported in some studies[38-40] was not corroborated in others.[33, 34, 41-43] Alternatively, one or more peaks have been proposed to account for a 'semi-ordered,' 'transition,' or 'intermediate' phase/region. Simanke et al. reject this possibility based on the idea that scattering from

such a phase would not be limited to any particular angular region in the WAXS patterns due to conformationally diffuse interfacial region between ordered and disordered phases.[33] Nonetheless, some groups maintain the existence of a semi-ordered phase that contributes one or two relatively narrow reflections. Sajkiewicz et al.[5] proposed the presence of a phase having intermediate properties to those of the crystalline and amorphous layers. As such, this intermediate phase was believed to contribute a hidden, relatively narrow peak to the WAXS intensity located between the amorphous halo and the (110) reflection. As would be expected, this peak was found to broaden and shift in angular position towards the amorphous halo with increasing SCB content and molecular weight (based on the fitting algorithm used).When two peaks have been used to account for the semi-ordered region, they have closely resembled the (110) and (200) orthorhombic reflections, but had lesser intensity and were shifted to lower q-values.[7, 34, 35, 37] These are referred to as '(110)' and '(200)', respectively, by Rabiej et al.[35] As an alternative explanation for the poor fit provided by the two-phase model, some authors suggest that a possible transition region between the crystalline and non-crystalline layers contributes to density heterogeneity in the amorphous halo which can be captured by an additional amorphous-halo-like scattering in a large angular range.[4, 36] The sensitivity of 2D correlation analysis to overlapping features makes it a well-suited technique to gain further insight into the possibility of a semi-ordered phase.

In the following, we examine the evolution of morphology during the crystallization of random copolymers (HPBDs) using conventional and heterospectral 2D correlation analysis. WAXS behavior of a homopolymer (HDPE) was also examined for comparison. Unique features corresponding to the development of different morphologies

(primary and secondary lamellae, fringed micelles) and the occurrence of physical processes (crystal growth, thermal contraction, etc.) are identified. The application of heterospectral analysis in the earliest stages of crystallization is used to comment on the dominant physical processes during the onset of crystallization.

4.2 EXPERIMENTAL METHODS

4.2.1 Materials

The materials used for the present study are the same hydrogenated polybutadienes (HPBDs) as described in the previous chapter (Section 3.2.1). Table 3.1 is reproduced for convenience as Table 4.1.

Table 4.1 Molecular characteristics of polyethylene materials examined. All values provided by ExxonMobil.

Polymer	Type	$M_{w,tot}$ (kg/mol)	PDI	$M_{w,b}$ (kg/mol)	$M_{w,a}$ (kg/mol)	Branches/ 1000 C[a]
L53	Linear	53	<1.05	53		19.2
L152	Linear	152	<1.05	152		19.5
S3	3-arm star	141	<1.05		47	18.9
H4	H-polymer	156	<1.05	112	11	26.3
HDPE	Linear	529	3.0	529		0.2

[a] obtained via ^{13}C NMR

4.2.2 X-ray Scattering

Morphology development during heating and cooling ramps (10 °C/min from 180 to 0 °C) was followed using wide and small angle x-ray scattering (WAXS and SAXS, respectively) as described in the previous chapter with scattering patterns collected every 2 °C (Section 3.2.2 of Chapter 3).

4.2.3 Computation

4.2.3.1 Conventional 2D Correlation Analysis

Two-dimensional (2D) correlation analysis of the x-ray scattering data was conducted using Noda's generalized method[19, 20] as described in Section 2.2.4 of Chapter 2. Discrete 'spectra' consisted of the Lorentz corrected SAXS and WAXS intensities, $J(q) = I(q)q^2$, as a function of the scattering vector, q. An exception was made in an examination of the onset of crystallization; here, the Lorentz correction does not apply because of the lack of a well-resolved scattering peak at the highest temperatures hence non-Lorentz corrected curves, $I(q)$, were analyzed.[44] The perturbation variable was temperature, as in Chapter 2. Correlation analysis was applied separately to scattering curves corresponding to primary-irreversible, secondary-irreversible, and reversible crystallization regimes (see previous chapter). Additionally, modified mean normalization was applied SAXS data as it has been observed to help discriminate overlapped peaks.[45] In this case, prior to calculation of the 2D correlation plots, individual scattering curves ($I_i(q) = I(q,T_i)$ for i = 1, 2, 3,…, m) were normalized for average intensity, $I_{i,mean}$, and maximum intensity, $I_{i,max}$:

$$I_{i,norm} = \frac{I_i}{I_{i,mean}{}^2 / I_{i,\max}}, \tag{4.1}$$

where

$$I_{i,mean} = \frac{1}{q_{\max} - q_{\min}} \int_{q_{\min}}^{q_{\max}} I_i(q)dq\,. \tag{4.2}$$

This pre-treatment accounts for differences in peak area and half width by approximating bands as Lorentzian peaks in order to minimize effects of strong intensity changes.[45] The

resulting scattering curves were examined to ensure no artificial peaks resulted from the normalization.[46-48]

4.2.3.2 Two-Dimensional Moving Window Analysis

While conventional 2D correlation analysis allows for the identification of overall trends in response to a perturbation, sometimes this results in omission of subtle aspects that are limited to a specific range of the perturbation variable. For example, minor intensity changes at high temperature may not be apparent if significant changes dominate at low temperatures. In this case, intensity changes as a function of the perturbation variable, T, of a large dataset ($I_i(q) = I(q,T_i)$ for $i = 1, 2, 3,\ldots, m$, represented schematically in Figure 4.1a) can be examined by the implementation of moving window 2D correlation (MW2D) analysis.[25, 49, 50] The synchronous 2D correlation spectrum is calculated for a subset or smaller 'window' of spectra ($I_i(q)$, $i = M,\ldots, M + \Delta M$, where $1 < M < M + \Delta M < m$) that is shifted sequentially by one spectrum through the full data set (Figure 4.1a,b). Here, subsets examined corresponded to 10 °C. For each window, a 1D spectrum is selected to be characteristic of the 2D spectrum (Figure 4.1c). The autocorrelation intensity (diagonal of the synchronous spectrum) is used in conventional MW2D, as it depicts the overall changes in intensity occurring simultaneously. When MW2D is used in conjunction with heterospectral analysis (see below), the autocorrelation intensity has little meaning, hence a specifically selected slice spectrum that represents the behavior of interest is used instead. The set of 1D spectra obtained from the window as it is shifted sequentially through the data set is plotted as a function of the perturbation variable, or in this case, temperature (Figure 4.1d).

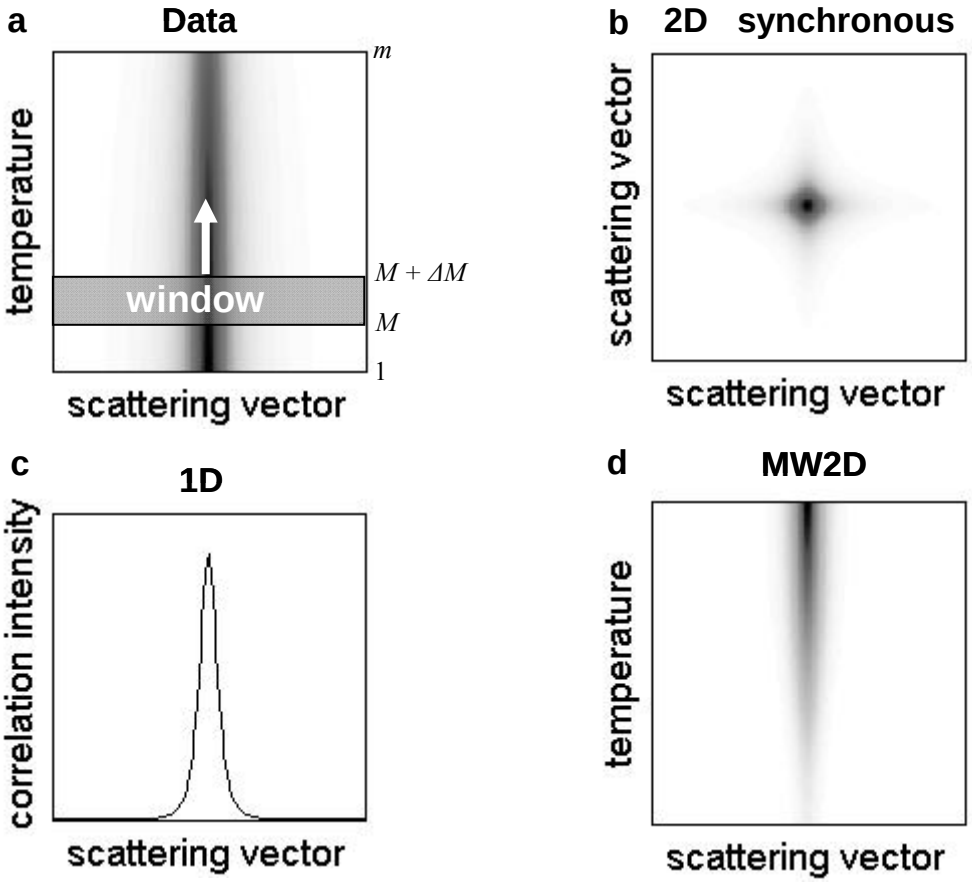

Figure 4.1 A schematic representation of 2D moving window analysis. **a)** A 'window' from the full dataset is selected and shifted sequentially through the set. **b)** For each window, a 2D synchronous spectrum is calculated. **c)** A 1D spectrum is selected to represent the 2D spectrum in **b**. **d)** These 1D spectra for each window plotted as a function of the perturbation variable (i.e., temperature).

4.2.3.3 Heterospectral Correlation Analysis

Simultaneous changes in SAXS and WAXS occurring as a consequence of the same physical processes are revealed by 2D heterospectral correlation analysis. Heterospectral correlation analysis identifies simultaneous changes in the system observed by two different probes under the same perturbation: Lorentz corrected SAXS ($J_{SAXS,i}(q) = J_{SAXS}(q,T_i)$, i = 1,2,3,…, m) and WAXS ($J_{WAXS,i}(q) = J_{WAXS}(q,T_i)$, i = 1,2,3,…, m) curves collected during temperature ramps. Dynamic scattering curves for both SAXS and

WAXS intensities, $\tilde{J}_i(q)$, are calculated with respect to the temperature-averaged spectrum:

$$\tilde{J}_i(q) = J_i(q) - \bar{J}(q), \tag{4.3}$$

where

$$\bar{J}(q) = \frac{1}{m}\sum_{i=1}^{m} J(q, T_i). \tag{4.4}$$

The synchronous 2D heterospectral correlation spectrum is calculated as

$$\Phi(q_1, q_2) = \frac{1}{m-1}\sum_{i=1}^{m} \tilde{J}_{SAXS,i}(q_1) \cdot \tilde{J}_{WAXS,i}(q_2). \tag{4.5}$$

The asynchronous spectrum was not considered because it lacks well-established interpretation.[17, 18, 31]

Additionally, the onset of crystallization was examined using a combination of 2D heterospectral correlation analysis in conjunction with MW2D. In this case, forgoing the Lorentz correction allowed us to include SAXS curves that lack a well-defined peak.[44] Two-dimensional hetero-spectra were calculated for data 'windows' corresponding to approximately 10 °C, as described above, in order to gauge simultaneous changes in SAXS and WAXS intensities early in the crystallization process. For the 1D representation of the 2D hetero-spectra, the correlation intensity corresponding to the (110) WAXS reflection was examined as a function of temperature.

For image presentation, contour levels were adjusted to exclude the bottom 5% of intensity values. Additionally, contour plots reveal relative intensities; therefore different figures have different contour levels in order to highlight the relevant features in each case. Unless otherwise stated, intensity values between different figures cannot be compared by the apparent relative intensity of features.

4.3 RESULTS AND DISCUSSION

In Chapter 3, we showed that morphology evolution during quiescent cooling and heating ramps can be characterized by two well-defined regimes: irreversible and reversible crystallization/melting.[3, 51-54] The irreversible crystallization regime occurs at higher temperatures relative to the reversible one and is marked by relatively large changes with temperature in morphological parameters (long period, L_p, crystallinity, X_c, and SAXS integrated intensity, Q), which exhibit a hysteresis upon cooling and heating (Figure 3.16 in Chapter 3). Irreversible crystallization of model random copolymers can be further divided into two regimes according to the degree of change of the morphological parameters: the 'primary-irreversible' regime, which exhibits the fastest changes in morphological parameters (Figure 3.16a,b in Chapter 3) and, at lower temperatures, 'secondary-irreversible' crystallization regime, which is characterized by slower changes in X_c and L_p and a broad maximum in Q (Figure 3.16a,c in Chapter 3). Reversible crystallization occurs at the lowest temperatures where morphological parameters during heating and cooling overlap and change mildly with temperature relative to the irreversible regimes (Figure 3.16a in Chapter 3). The WAXS and SAXS results for these regimes are well-suited for the application of 2D correlation analysis, with goals to both to elucidate features corresponding to specific morphology changes that are difficult to discern via traditional analysis and to establish characteristic 2D signatures of the three regimes, which correspond to the evolution of different morphology (primary and secondary lamellae, as well as fringed micelles).

4.3.1 WAXS

4.3.1.1 Polyethylene WAXS Features

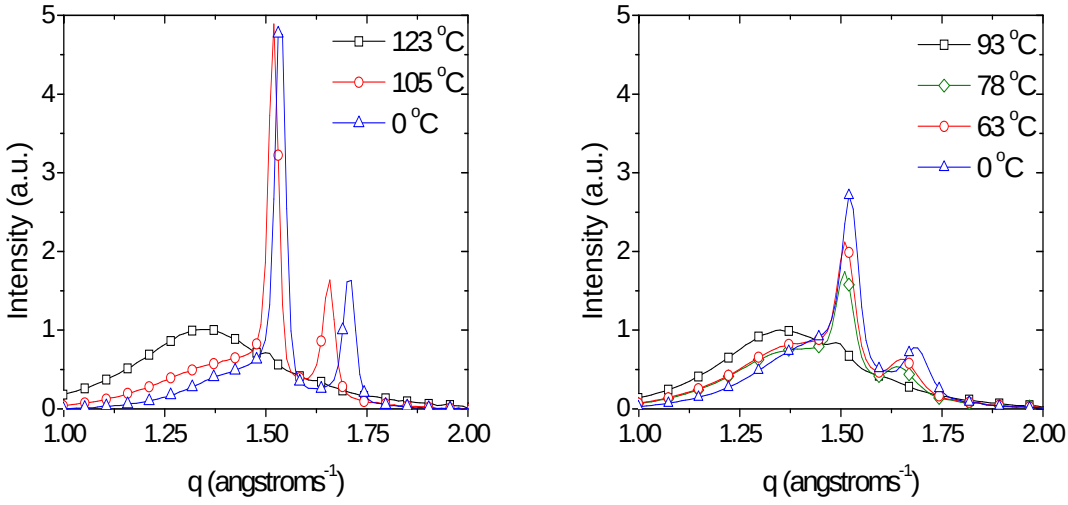

Figure 4.2 WAXS intensity during cooling at 10 °C/min at temperatures marking the bounds of different crystallization regimes for **a)** HDPE and **b)** L152 while cooling at 10 °C/min.

Examination of the WAXS crystallinity evolution through the analysis of two-dimensional correlation plots focuses on three salient WAXS features of polyethylene materials: the broad amorphous halo (centered at approximately 1.35 $Å^{-1}$) and the two most prominent crystalline reflections of the orthorhombic unit cell, which are due to the (110)-planes (near 1.5 $Å^{-1}$) and the (200)-planes (near 1.65 $Å^{-1}$) (Figure 4.2).

Figure 4.2 compares 1D WAXS curves at temperatures corresponding to the transitions between different crystallization regimes for HDPE and L152. HDPE develops almost all of its crystallinity via irreversible crystallization in the range between 123 and 105 °C as evidenced by large changes in intensity of the crystalline reflections (Figure 4.2a). Little change in the intensity of the crystalline peaks was observed between 105 and 0 °C, consistent with minimal crystallization occurring in the reversible regime

(Figure 4.2a). However, crystalline reflections are shifted to higher values of q at the end of the reversible regime (T = 0 °C) compared to at its beginning (T = 105 °C) as a consequence of thermal contraction.[55, 56]

Behavior of L152 is more complex and is characterized by 4 temperatures of interest that define its three crystallization regimes: primary-irreversible (93 to 78 °C), secondary-irreversible (78 to 63 °C), and reversible (below 63 °C). Appreciable crystallinity develops during all three regimes marked by the increase in magnitude of the crystal reflections. An increase in width of the crystal reflections is also observed and is a consequence of SCB content. At lower temperatures, crystallization of shorter ethylene sequences leads to more chain defects (i.e., short-chain branches) encountered by the crystal growth front. The result is a decrease in coherence of unit cells manifested as a broadening of the crystal reflections.

Similar to HDPE, L152 crystal reflections shift to higher q-values with decreasing temperature as the result of thermal contraction but their intensities change as well. Moreover, L152 (Figure 4.2b) exhibits crystalline reflections that are shifted to slightly lower q-values relative to HDPE; for example, the (200) reflection at 0 °C is located at 1.68 $Å^{-1}$ for L152 versus 1.70 $Å^{-1}$ for HDPE. This is a result of SCB-induced expansion of the orthorhombic unit cell—a phenomenon frequently observed in prior literature on ethylene copolymers.[4, 5, 33, 57-63] Although the reason for this effect is obvious in the case of methyl groups that are incorporated into the crystal lattice,[64] ethyl, butyl, and hexyl branches also have a small but noticeable effect attributed to the strain they induce by crowding at the interface of thin crystals.[57, 62]

A final important feature is the increase in scattering intensity in a small *q*-range near 1.45 $Å^{-1}$ during secondary-irreversible crystallization (compare 78 with 63 °C in Figure 4.2) and reversible crystallization (compare 0 with 63 °C in Figure 4.2). In contrast to HDPE, L152 does not exhibit a monotonic decrease in amorphous halo scattering with decreasing temperature, but rather a pronounced change in shape. Some authors attribute this shape change to the presence of a third phase having intermediate properties between crystalline and amorphous phases.[5] In light of this and other theories, scattering in this region is further explored using 2D correlation analysis.

4.3.1.2 Crystallization of Homopolymers

Since HDPE has only two crystallization regimes: (1) irreversible crystallization that occurs in the range of 123 to 105 °C and accounts for approximately 85% of crystallinity developed during cooling to 0 °C (Figure 3.7 in Chapter 3) and (2) reversible crystallization in the range of 105 to 0 °C, two-dimensional correlation analysis was applied to WAXS spectra in these two temperature ranges. As mentioned previously, a secondary-irreversible regime was not present.

Irreversible Crystallization

Irreversible crystallization of HDPE is characterized by a strong increase in the amount of crystalline material, which is manifested as an increase in diffracted intensity of the (110) and (200) crystalline reflections. Consequently, the 2D synchronous pattern is dominated by two strong autopeaks (located along the diagonal) at approximately 1.5 and 1.65 $Å^{-1}$ associated with monotonic changes in the (110) and (200) reflections

(Figure 4.3a). In addition, since the intensities of both peaks increase as the result of the same physical process—the formation of orthorhombic unit cells—the cross peaks at (1.52 $Å^{-1}$, 1.66 $Å^{-1}$) and (1.66 $Å^{-1}$, 1.52 $Å^{-1}$), which measure the extent to which changes in both peaks occur simultaneously are also strong. The sign of these cross peaks is positive, consistent with the intensity change of (110) and (200) peaks occurring in the same direction (i.e., both increasing during crystallization).

Formation of crystallites inherently consumes the subcooled melt, both by organizing polyethylene strands into crystals and by altering the non-crystalline material that is trapped between lamellae. The corresponding amorphous halo is very broad, so its change in peak intensity is much weaker than that of the crystalline reflections (approximately 11% as large as the change in the intensity of the (110) reflection). Consequently, the autocorrelation peak associated with the amorphous halo is extremely weak compared to crystalline peaks and is below the contour threshold of the synchronous pattern in Figure 4.3a. Indeed, compared to the (110) peak, the halo autocorrelation intensity is only $(11\%)^2 \approx 1\%$, due to the quadratic nature of 2D correlation, and is practically invisible. Correlation peaks between the amorphous halo and the crystalline reflections, on the other hand, are readily visible on this scale as negative cross peaks: their magnitude scales as the product of the amount of the change in the amorphous halo (weak) and the change in the respective crystalline peak (strong). The shape of these features is elongated due to the breadth of the amorphous halo and the sharpness of the diffraction peaks. Their negative sign indicates that crystalline peaks change in the opposite direction from the amorphous halo consistent with the growth of crystals occurring at the expense of non-crystalline material, in accord with physical interpretation of crystallization.

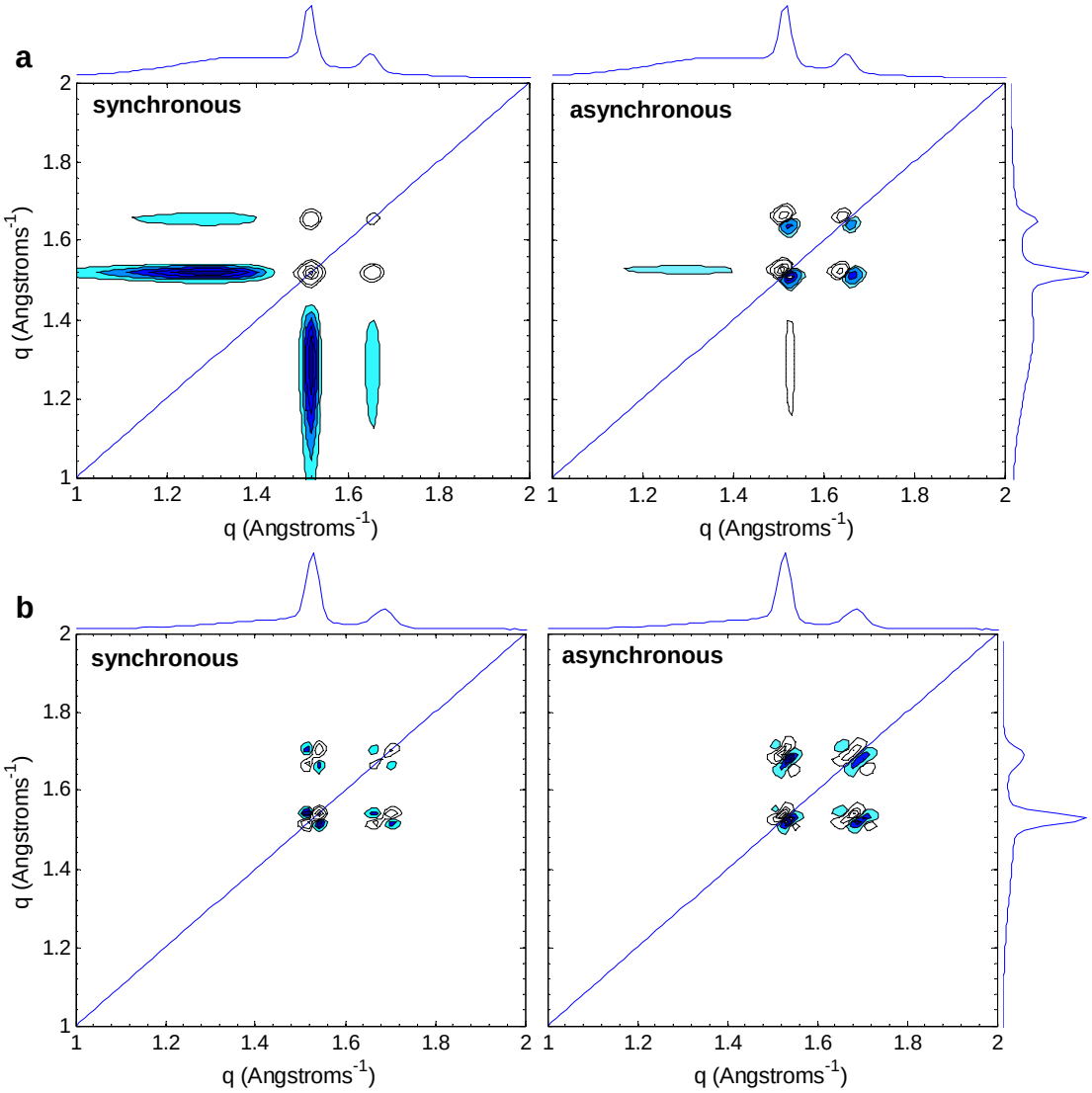

Figure 4.3 2D synchronous (left) and asynchronous (right) correlation plots derived from Lorentz corrected WAXS curves collected during **a)** irreversible (105 °C < T < 123 °C) and **b)** reversible (0 °C < T < 105 °C) crystallization of HDPE occurring during cooling at 10 °C/min. Positive and negative contours are shown as open and filled, respectively. Averaged 1D scattering profiles are shown on the sides.

The asynchronous plot reveals that crystallization is not the only physical process that occurs during cooling. Different physical processes can be identified by intensity changes that are temporally separated, the extent of which can be observed in the corresponding asynchronous plots. In the case of HDPE undergoing irreversible crystallization (105 °C < T < 123 °C), the asynchronous plot displays tightly-packed pairs of cross peaks

located at the vertices of the correlation square defined by the crystalline reflections: (1.52 $Å^{-1}$, 1.52 $Å^{-1}$), (1.66 $Å^{-1}$, 1.66 $Å^{-1}$), (1.52 $Å^{-1}$, 1.66 $Å^{-1}$), and (1.66 $Å^{-1}$, 1.52 $Å^{-1}$). A doublet corresponding to a crystalline reflection can arise either from overlapping peaks changing at different rates (e.g., different crystal morphs) or from a shift in the position of a single peak. Given that the orthorhombic crystal morph is the only one expected under these conditions,[65] the doublets here are attributed to mild changes in peak position,[66, 67] which is a consequence of thermal contraction. The position of the doublet attributed to the (200) reflection at (1.64 $Å^{-1}$,1.66 $Å^{-1}$) can be interpreted as a shift in position of this reflection from approximately 1.64 $Å^{-1}$ to 1.66 $Å^{-1}$; the corresponding 0.09 Å change in the unit cell parameter, *a*, is consistent with thermal contraction of the *a*-axis of the polyethylene crystal in the temperature range associated with irreversible crystallization.[55] The doublets appearing at the cross positions near (1.52 $Å^{-1}$, 1.66 $Å^{-1}$) are a consequence of the shape of the features along the diagonal. The intensities of these doublets are an order of magnitude lower than corresponding synchronous peaks indicating that peak shifting is a secondary process to crystal formation.

Weak cross peaks can also be observed between the amorphous halo (1.2–1.4 $Å^{-1}$) and the (110) reflection (1.52 $Å^{-1}$). The corresponding cross peak between the amorphous halo and the (200) reflection (1.2–1.4 $Å^{-1}$ and 1.66 $Å^{-1}$) is too weak and is not observed in Figure 4.3 due to the contour threshold. These cross peaks are consistent with the change in the amorphous halo exhibiting slight temporal separation from the growth of crystalline peaks. Following Noda's rules for the determination of sequential order of intensity changes,[68] it can be determined that change in the amorphous halo precedes the growth of

crystalline reflections. This observation can be explained by thermal contraction of the polyethylene melt prior to significant crystal formation.[4]

Reversible Crystallization

While crystallinity development is the dominant physical process during irreversible crystallization, only approximately 15% of total crystallinity develops in the range from 105 to 0 °C corresponding to the reversible regime. This difference is apparent in the 2D correlation patterns which exhibit clusters of peaks corresponding to the crystalline reflections of HDPE, which exhibit characteristic features of a shift in peak position (Figure 4.3b). The "clover-leaf" patterns observed in the synchronous spectrum (positive autopeaks with negative cross peaks) indicate that both the (110) and (200) reflections undergo simultaneous decrease and increase in intensity on either side of the peak. While this could suggest the presence of overlapping peaks, the corresponding "butterfly" patterns in the asynchronous plot (Figure 4.3b, right) are characteristic of well-defined peak shifts of both of these crystalline reflections.[18, 66, 69, 70] These well-defined patterns indicating position shifts are evident because they are not convoluted by strong changes in intensity like during irreversible crystallization (see Figure 4.2a). When such patterns are present, the two autopeaks of the clover-leaf pattern corresponding to a single reflection indicate the starting and ending peak positions; for the (200) reflection, these positions are 1.66 and 1.70 $Å^{-1}$, respectively, which is confirmed by the 1D WAXS curves (Figure 4.2). The sign of the 'wing' below the diagonal in the asynchronous butterfly patterns indicates that the positions of crystalline reflections shift in the direction from smaller to larger q-values, in agreement with thermal contraction.[18] The peak shift of the (200) reflection corresponds to a contraction in a of approximately 0.36 Å, which

is again consistent with thermal effects expected across the 105 °C range of reversible crystallization.[55, 71, 72] It is reassuring to note that the positions of the crystalline reflections, as determined by 2D correlation analysis, are continuous through the transition between the two crystallization regimes. The symmetry of the clover patterns is consistent with only minor changes in peak intensity during the shift, indicating that thermal contraction of the crystal phase is the dominant physical process in this regime.

4.3.1.3 Crystallization of Random Copolymers

The crystallization of L152 and the other HPBD materials investigated can be separated into three regimes: (1) primary-irreversible crystallization (93 to 78 °C), which accounts for 63% of the total crystallinity at 0 °C, (2) secondary-irreversible crystallization (78 to 63 °C), which accounts for 13% of total crystallinity at 0 °C, and (3) reversible crystallization (63 to 0 °C), which accounts for 24% of total crystallinity developed during cooling to 0 °C (Figure 3.7 in Chapter 3).

Primary-Irreversible Crystallization

The synchronous spectrum of L152 during primary-irreversible crystallization occurring between 93 and 78 °C (Figure 4.4a, left) displays similar features to that of HDPE (Figure 4.3a, left) with the exception of an additional autopeak corresponding to the amorphous halo near 1.3 $Å^{-1}$. The latter should be not interpreted as a greater change in the amorphous halo in L152 compared with HDPE; rather, it is a consequence of the much weaker (110) and (200) diffraction peaks of L152 relative to HDPE (Figure 4.2). The crystalline reflections in this regime are located at almost the same peak position as

HDPE ((1.51 $Å^{-1}$, 1.51 $Å^{-1}$) for the (110) reflection and (1.66 $Å^{-1}$, 1.66 $Å^{-1}$) for the (200) reflection) despite the difference in temperature (~30 °C) at which primary-irreversible crystallization occurs (78 to 93 °C for L152 versus 105 to 123 °C for HDPE). This is explained by the thermal contraction of the unit cell being offset by the effect of SCB, which is know to cause expansion of the unit cell.[4, 5, 33, 57-63]

Similar to HDPE, the asynchronous features of L152 are over an order of magnitude smaller than synchronous ones (Figure 4.4a, right). However, L152 and HDPE asynchronous plots exhibit marked differences that are the result of an increased relative contribution of the amorphous halo in the case of L152. Correlation between the amorphous halo and the (110) reflection reveals a pattern resembling an asymmetric, highly elongated doublet near (1.49 $Å^{-1}$, 1.15 $Å^{-1}$) and (1.52 $Å^{-1}$, 1.35 $Å^{-1}$) consistent with temporal separation between changes in the non-crystalline and crystalline phases. The fluctuating outlines of the features corresponding to the amorphous halo indicate that it is barely above the noise, hence the temporal separation between changes in the crystalline and non-crystalline phases is mild.

The crystalline reflections can again be recognized in the asynchronous plot by the appearance of doublets. The doublet corresponding to the (110) reflection at (1.52 $Å^{-1}$, 1.49 $Å^{-1}$) is tightly spaced, similar to the case of HDPE, indicating minor changes in the (110) peak position consistent with thermal contraction. In contrast, the feature corresponding to the (200) reflection is further offset from the diagonal at (1.66 $Å^{-1}$, 1.62 $Å^{-1}$). This feature cannot be fully explained by thermal contraction because a 0.04 $Å^{-1}$shift in the peak position corresponds to too large a difference in unit cell dimensions (almost 0.18 Å difference in *a*) in this 15 °C range.[73, 74]

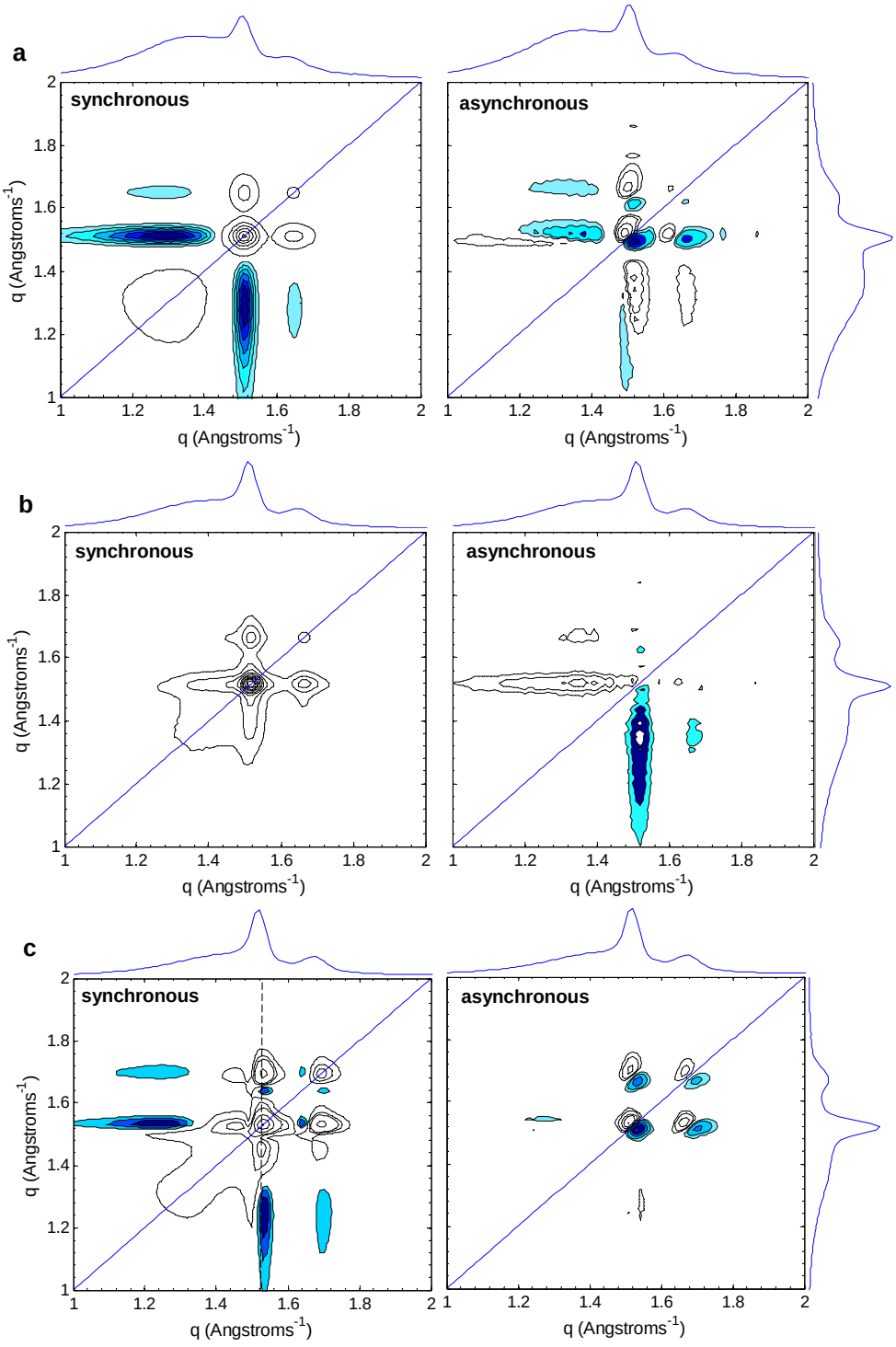

Figure 4.4 2D synchronous (left) and asynchronous (right) correlation plots derived from Lorentz corrected WAXS curves collected during cooling at 10 °C/min in the **a)** primary-irreversible (78 °C < T < 93 °C) **b)** secondary-irreversible (63 °C < T < 78 °C) and **c)** reversible (0 °C < T < 63 °C) regimes of L152. Positive and negative contours are shown as open and filled, respectively. Averaged 1D scattering profiles are shown on the sides.

Alternatively, one may argue that the feature corresponding to the (200) reflection reflect temporally separated changes at 1.62 and 1.66 $Å^{-1}$ and are therefore the result of two scattering populations. One may assign the two overlapped peaks as the crystalline (200) reflection centered at 1.66 $Å^{-1}$ and the '(200)' semi-ordered phase reflection centered at 1.62 $Å^{-1}$.[35] In this scenario, the tightly-spaced (110) doublet would also be attributed to changes in the (110) crystalline reflection and the '(110)' reflection of the semi-ordered phase, which are closer spaced at 1.52 and 1.49 $Å^{-1}$, respectively.

On the other hand, the unusual magnitude and position of the (200) reflection may be attributed to a convolution of its behavior with changes in the broad amorphous halo having comparable magnitude. In addition to thermal contraction of the non-crystalline material (shifting the halo to large q), during crystallization of HPBDs, the amorphous halo changes shape due to the enrichment of butyl branches in the non-crystalline regions as they are rejected from the crystals. This shape change results in comparable changes in magnitude between the amorphous halo and the (200) reflection. Hence, the decrease in the amorphous halo during crystallization convoluted with the change in position of the (200) reflection results in an altered 2D feature.

Secondary-Irreversible Crystallization

Crystallization in the secondary-irreversible regime is characterized by an overall increase in intensity occurring both in the crystalline reflections and the amorphous halo immediately adjacent to the (110) peak (Figure 4.4b, left). In addition to the familiar autopeaks and cross peaks associated with the (110) and (200) crystalline reflections at 1.52 and 1.67 $Å^{-1}$, analogous to those in Figure 4.3a and Figure 4.4a, a change in shape of the amorphous halo combined with a minimal change in crystallinity (13% in this re-

gime) resulted in a qualitatively different 2D pattern. In contrast to the primary-irreversible regime, negative features corresponding to the decrease in the amorphous halo as a consequence of the development of crystallinity were not observed. Instead, the magnitude of the amorphous halo increased in the *q*-region adjacent to the (110) reflection near 1.35–1.46 $Å^{-1}$. A scattering peak in this region was suggested to correspond to an 'intermediate' phase by Sajkiewicz et al.[5] On the other hand, this observation is also consistent with increased packing density of a fraction of the non-crystalline regions resulting in a heterogeneous density distribution.[4, 36]

The asynchronous plot is dominated by features corresponding to the amorphous region below 1.46 $Å^{-1}$ and the crystalline reflections (Figure 4.4b, right). Although the temperature range corresponding to secondary-irreversible crystallization is the same as for primary-irreversible crystallization (15 °C), the asynchronous spectrum here lacks elongated doublets corresponding to thermal contraction of the crystalline phase (compare with Figure 4.4a, right). Instead, a (200) feature is too weak to see and the (110) doublet (which is not resolved from the amorphous feature) is barely above the noise. These observations highlight the different physical processes that dominate these crystallization regimes. We speculate that the secondary lamella forming in this lower-temperature regime suffer more interfacial stress due to the accumulation of SCB at their crystal faces leading to formation of expanded unit cells.[4, 5, 33, 57-63] This effect counters the decrease in the unit cell due to thermal contraction resulting in little change in position of the diffraction peaks, which is confirmed by the 1D WAXS curves (Figure 4.2b). Ultimately, the relative intensity of the asynchronous compared to the synchronous fea-

tures is even weaker in the secondary-irreversible than in the primary-irreversible regime (i.e., the changes in $I(q)$ occur very nearly simultaneously).

If one accepts that a semi-ordered phase develops during primary-irreversible crystallization, then it can account for the growth of scattering intensity in the region of 1.35–1.46 $Å^{-1}$ during crystallization. However, the jump of this reflection to lower q-values (from 1.49 $Å^{-1}$ during primary-irreversible crystallization) is unlikely. The positive cross peaks between the two crystalline reflections at (1.61 $Å^{-1}$, 1.52 $Å^{-1}$) can be attributed to growth in the '(200)' semi-ordered phase reflection, which is located at the same position as in the primary-irreversible regime. Alternatively, an increase in scattering of the amorphous halo may be a consequence of the increase in density of non-crystalline regions with decreasing temperature.[37] This increase scattering is unevenly distributed (greatest near 1.35–1.46 $Å^{-1}$) due to heterogeneities arising within the non-crystalline regions as a result of its enrichment with butyl groups immediately adjacent to the crystal surface and consequent crowding of pinned chains that are incapable of crystallization. These alternative scenarios are further discussed in Section 4.3.1.4.

Reversible Crystallization

The significant increase in crystallinity that is unique to reversible crystallization of L152, and the other HPBDs examined, is apparent in the synchronous plot in the familiar autopeaks corresponding to the (110) and (200) crystalline reflections at (1.53 $Å^{-1}$, 1.53 $Å^{-1}$) and (1.70 $Å^{-1}$, 1.70 $Å^{-1}$). These peaks are shifted to larger q-values relative to crystallization in the irreversible regimes as a consequence of thermal contraction (Figure 4.4c, left). Thermal contraction continues in the range below 63 °C corresponding to reversible crystallization resulting in the elongated doublets in the asynchronous plot

(Figure 4.4c, right). These features are similar to those observed during irreversible crystallization of HDPE (Figure 4.3a, right) and are consistent with peak shifting occurring simultaneously with more pronounced changes in intensity.

As discussed previously, all diffraction features shift to higher values of q through a decrease of intensity at low q-values and increase of intensity at high q-values, which can be seen from 1D WAXS curves at two different temperature in this regime in Figure 4.2b (at the beginning at T = 63 °C and at T = 0 °C). The autopeaks in the synchronous plot corresponding to the diffraction peaks resemble triangles as a consequence of the increasing breadth of the crystalline reflections, which is the result of crystallization of random copolymers at low temperatures (Figure 4.2b). Increased width of the diffraction peaks results from incoherent growth of unit cells as more chain defects are encountered during crystallization at low temperatures. This effect is manifested as increasing intensity on the right side (high-q side) of the crystalline reflections and corresponding triangular shape of 2D synchronous features. This shape is mirrored by the corresponding cross peaks since both crystalline reflections change simultaneously.

To further appreciate the richness of the 2D synchronous plot in the reversible regime, it is instructive to consider selected section through the plot. In particular, a section of $I(q_1,q_2)$ holding q_1 files at the (110) diffraction peak, such that $q_1 = q_{(110)}$, is indicated by the dashed like in Figure 4.4c. Moving along the dashed line from high q to low q (Figure 4.5c) there is a strong positive peak, a shallow negative interval, a shoulder leading up to the strong (110) autopeak, a resolved positive peak, and a broad negative feature. These features are compared with the temperature-averaged intensity in this regime

($\bar{I}(q)$, analogous to eq 4.4; Figure 4.5a) and the intensity pattern along the diagonal of the 2D synchronous plot referred to as the autocorrelation intensity (Figure 4.5b).

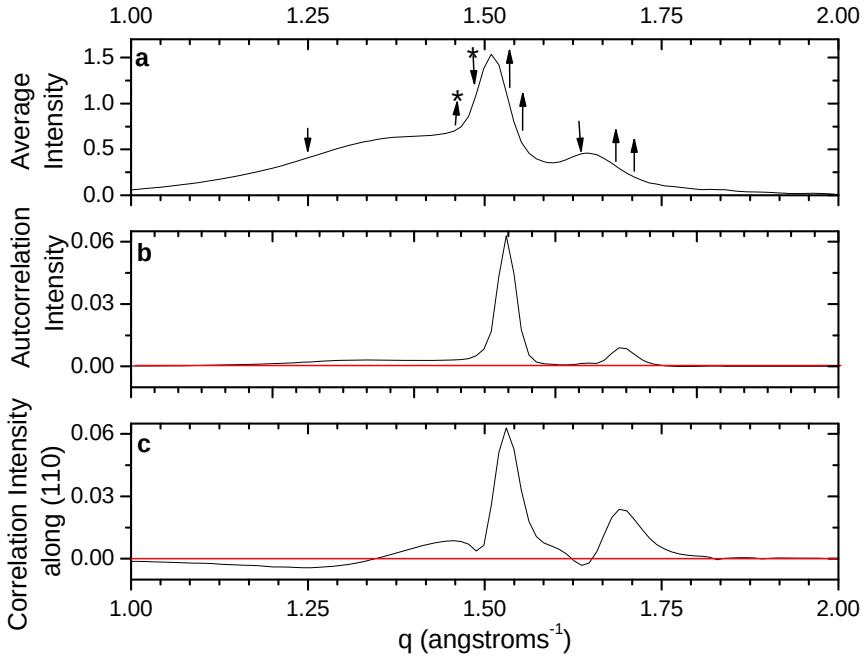

Figure 4.5 WAXS data for reversible crystallization of L152: **a)** average curve with arrows indicating direction of intensity change, **b)** intensity along the diagonal of the synchronous plot, and **c)** synchronous correlation intensity along the (110) reflection marked by dashed line in Figure 4.4c, left.

The strongest feature in Figure 4.5c is attributed to the (110) autopeak (where the dashed line crossed the diagonal in Figure 4.4c), which is confirmed by its correspondence in position with the peak in the autocorrelation spectrum (Figure 4.5b). This peak is offset to high-*q* relative to the (110) peak in the average intensity (Figure 4.5a), since it reflects the *increase* of intensity during cooling from 63 to 0 °C. This increase occurs mainly on the high-*q* side of the diffraction peaks (indicated by upward arrows on the

high-q side of both diffraction peaks in Figure 4.5a) due to the simultaneous thermal contraction of previously formed crystallites and the formation of new ones.

The second strongest feature in the correlation intensity along $q_{(110)}$ occurs at 1.70 $Å^{-1}$and is readily assigned to the positive correlation between growth of intensity on the high-q side of both the (110) and (200) peaks; it is a section through the (110)/(200) cross peak above the diagonal in Figure 4.4c where the dashed line passes through it.

There is a third positive peak in the correlation intensity along $q_{(110)}$ at 1.46 $Å^{-1}$ in Figure 4.5c. Like the (110)/(200) cross peak, the positive sign of this peak indicates an increase of intensity at 1.46 $Å^{-1}$ that coincides with the increase in intensity on the high-q side of the (110) peak. Due to both its position and breadth, this feature is attributed to the non-crystalline material.

There are also two negative intervals in the correlation intensity with the (110) diffraction peak: a broad one at $q < 1.34$ $Å^{-1}$ and a narrow one at 1.64 $Å^{-1}$. The former is assigned to the decrease in intensity in the amorphous halo at $q < 1.34$ $Å^{-1}$ (compare 63 to 0 °C in Figure 4.2b and observe where the dashed line in Figure 4.4c cuts through the elongated native feature in the synchronous plot). The latter is attributed to the substantial shift of the (200) reflection to higher q-values as a consequence of thermal contraction, resulting in a decrease of intensity on the low-q side of the (200) peak (see downward arrow in Figure 4.5c at 1.64 $Å^{-1}$). A similar negative feature is expected on the low-q side of the (110) peak also. Instead, the decrease of the diffracted intensity at 1.49 $Å^{-1}$ due to thermal contraction (manifested by the local minimum in Figure 4.5c) is offset by the increase of scattered intensity in the broad range around 1.46 $Å^{-1}$ (see arrows marked with asterisks in Figure 4.5a).

The simultaneous occurrence of the change in non-crystalline scattering as crystallites form suggests that the formation of crystals alters the structure in adjacent non-crystalline material. The effect has negligible time lag (very weak signatures in the asynchronous plot in Figure 4.4c, right), suggesting that the effect is local; as reversible crystal form, they perturb the non-crystalline structure in their immediate vicinity. This is consistent with the physical interpretation of crystallization at low temperatures, which results in excessive crowding of butyl groups at the crystal surface resulting in greater constraint of the non-crystalline regions compared to higher temperatures.

4.3.1.4 Searching for a Semi-Ordered Phase

The existence of a semi-ordered phase that contributes relatively narrow reflections to WAXS has been suggested in prior literature in an attempt to improve the calculation of crystallinity from 1D spectra.[5, 7, 34, 35, 37] However, evidence in the form of a resolved feature of such a phase has never been observed in 1D scattering curves. The enhancement of spectral features possible through 2D correlation analysis makes it a useful technique to determine the existence of a semi-ordered phase.

All three crystallization regimes (primary-irreversible, secondary-irreversible, and reversible) exhibited features that could be construed as evidence of a semi-ordered phase. Cross correlation features in different regimes indicated changes in WAXS near 1.61–1.64 $Å^{-1}$ (at the low-q side of the (200) reflection) and changes in the region near 1.46 and 1.49 $Å^{-1}$ (adjacent to the (110) reflection), which one might assign to the '(200)' and '(110)' semi-ordered reflections, respectively.[35]

However, our analysis of the 2D correlation spectra forces us to reject this hypothesis of a semi-ordered phase resembling the crystalline phase. First of all, even employing the normalization schemes that are known to enhance spectral features (see Table 2.1 of Section 2.2.4) failed to resolve any autopeaks near 1.46–1.49 $Å^{-1}$ and 1.61–1.64 $Å^{-1}$.[45, 75-77]

Second, an effort was made to reconcile the changes in the WAXS in the three crystallization regimes. The three crystallization regimes exhibit (1) increases near 1.49 and 1.61 $Å^{-1}$ during primary-irreversible crystallization, (2) increases near 1.46 and 1.61 $Å^{-1}$ during secondary-irreversible crystallization, and (3) an increase at 1.46 $Å^{-1}$ but a decrease at 1.64 $Å^{-1}$ during reversible crystallization. The shift of the presumed '(110)' peak to lower q between the primary- and secondary- irreversible regimes (1.49 versus 1.46 $Å^{-1}$, respectively) without a corresponding shift in '(200)' as well as opposite changes in intensity of the two features during reversible crystallization defies a unified explanation in terms of a distinct, semi-ordered phase. Thus, the observed changes in the non-crystalline regions of WAXS do not support this hypothesis.

Alternatively, the changes in the non-crystalline regions of WAXS patterns may be explained by such well-established physical phenomena as thermal contraction, the loss of coherence in unit cell growth of copolymers at low temperatures, and crystallization-induced heterogeneity in the density distribution of the amorphous halo. The latter phenomenon is a consequence of the crystallization of HPBDs, which results in the enrichment of the non-crystalline regions closest to crystal faces with the rejected butyl groups and the shortest ethylene sequences. In contrast to HDPE, which crystallizes by chain folding with frequent nearby re-entry of the chain into the crystal (Figure 4.6a),

crystallization of HPBDs incorporates 'crystalline stems' that are usually delimited by butene units, resulting in strongly reduced probability of nearby re-entry (Figure 4.6b). The result is extreme crowding of chains at the crystal surface, which in addition to localized butene concentration and thermal contraction of these non-crystalline regions, can explain the change in the shape and position of the amorphous halo.[33, 36] Therefore, we favor the interpretation of McFaddin et al.[4] that attributes observed changes in the non-crystalline WAXS during crystallization to density heterogeneities rather than a semi-ordered phase.

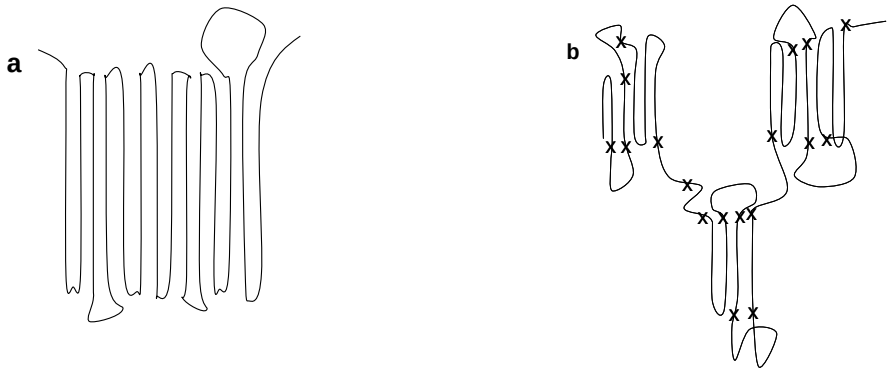

Figure 4.6 Schematic representation of crystallization of **a)** homopolymers and **b)** random copolymers.

4.3.2 SAXS

4.3.2.1 Crystallization of Random Copolymers

Two-dimensional correlation analysis provides an opportunity to examine the complex SAXS behavior of polyethylenes containing short-chain branches, which exhibit significant variation with temperature (Figure 3.9 in Chapter 3).[6, 43, 78-80] The three regimes of crystallization exhibited by HPBD materials are apparent in the evolution of Lorentz-corrected SAXS curves during cooling of L152 (Figure 4.7). Irreversible crystallization at high temperatures (primary-irreversible regime, dashed lines in Figure 4.7) is

characterized by an overall increase in the scattering power and a shift in the peak position to larger values of q. At intermediate temperatures (secondary-irreversible regime, solid lines in Figure 4.7), overall scattering power stays relatively constant while the peak position continues its shift. In the reversible regime at lower temperatures (dotted lines in Figure 4.7), the overall scattering power decreases while the peak position shifts further and broadens. It is important to note that in each regime, the change in the peak position and shape (magnitude and width) is monotonic, enabling the application of Noda's rules for sequential order determination based on asynchronous spectra.[68] Each regime is marked by unique signatures in the 2D correlation plots corresponding to the changes in the nanoscale structure during crystallization.

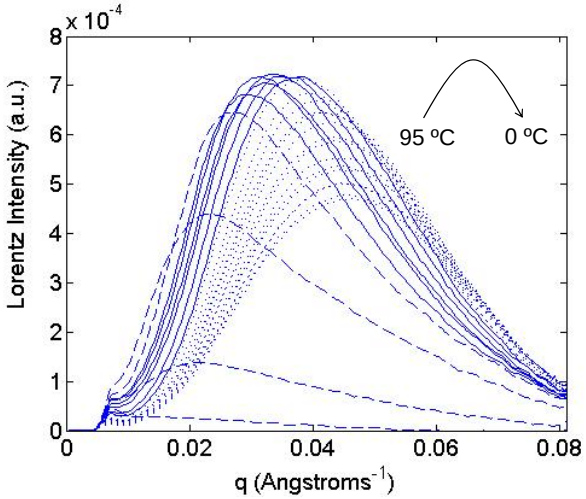

Figure 4.7 Lorentz-corrected SAXS of L152 during cooling at 10 °C/min exhibiting primary-irreversible (dashed lines), secondary-irreversible (solid lines), and reversible (dotted lines) regimes.

Primary-Irreversible Crystallization

The change in scattering power dominates both the synchronous and asynchronous plots during primary-irreversible crystallization of L152 (Figure 4.8a). The triangular shape of the solitary autopeak, whose center coincides with the peak of the average

scattering curves in this regime (above and beside Figure 4.8a), is consistent with an overall increase in scattering across a broad q-range. This synchronous feature can be interpreted as the formation of lamellae with a broad distribution of long periods centered near 22 nm. The asynchronous plot contains an elongated feature, the sign of which below the diagonal is consistent with growth of intensity at large q-values ($q > 0.02$ Å^{-1}) lagging that at low q-values ($q \sim 0.017$ Å^{-1}). This pattern—negative peak centered at (0.017 Å^{-1}, 0.031 Å^{-1})—indicates that the broad distribution of long periods arises through the initial formation of lamellae with an average long period of approximately 37 nm followed by the formation of a distribution of lamellae centered around 20 nm. The latter population has a distribution approximately twice as broad as the former population as indicated by the shape of the asynchronous cross peak.

A strictly positive change in scattering intensity at all q-values is consistent with the formation of primary lamellae propagating into unconstrained melt, as suggested in Chapter 3. The formation of lamellae with different characteristic length scales is a consequence of the ethylene sequence length distribution (ESLD). Initially, at the highest temperatures of this regime, only the longest ethylene sequences can crystallize. Due to the homogenous SCB distribution, although the number of these long sequences is small, they can be found in almost every chain. The crystallization of these sequences results in the majority of chains being pinned to crystal surfaces (even at low crystallinity), limiting their crystallization at elevated temperatures and resulting in large non-crystalline regions. As temperature decreases, progressively shorter-ethylene sequences can participate involving a larger percentage of each polymer chain. Hence, the non-crystalline layers decrease, resulting in a smaller long period.

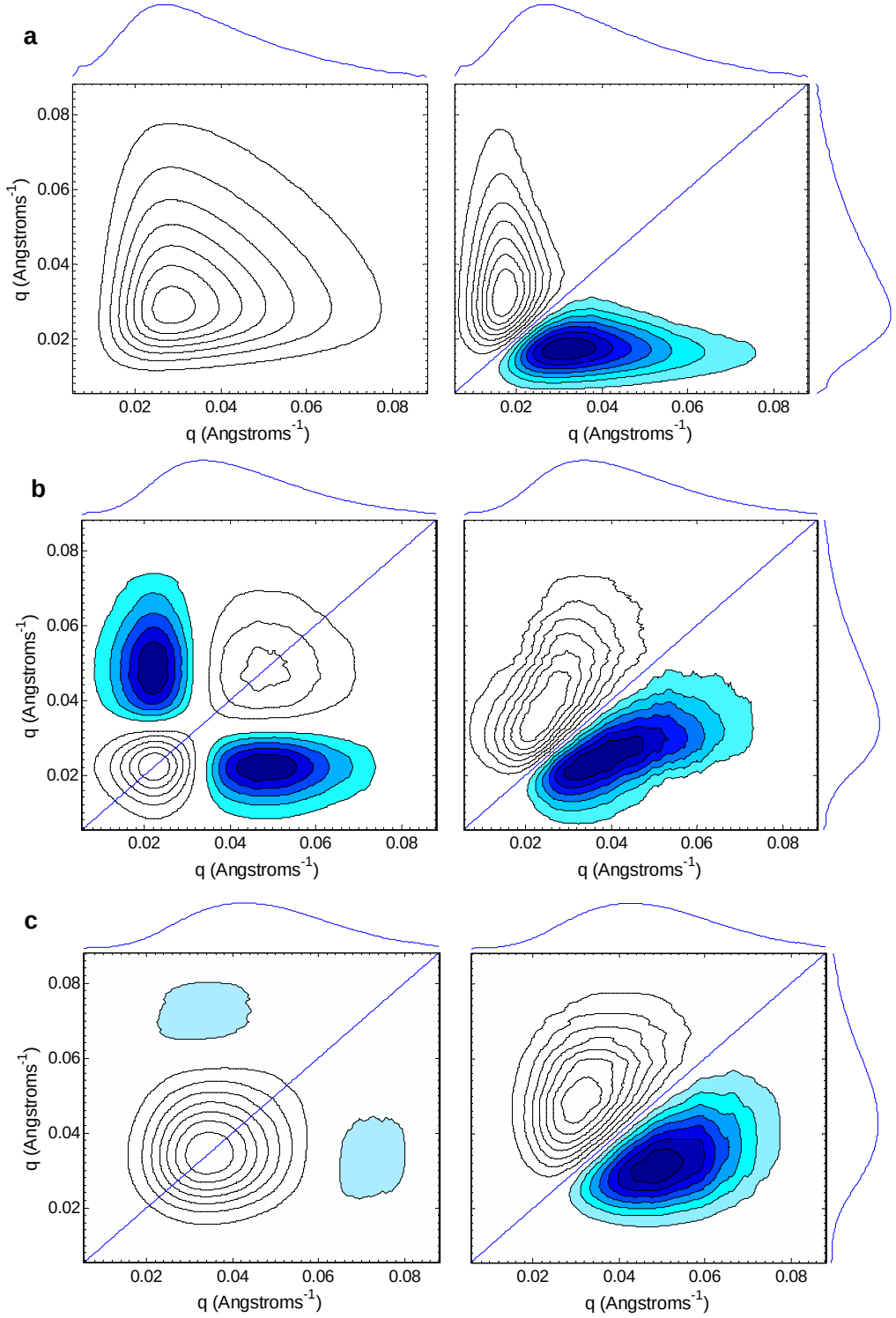

Figure 4.8 2D synchronous (left) and asynchronous (right) correlation plots computed from Lorentz-corrected SAXS curves collected in **a)** primary-irreversible (78 °C < T < 93 °C), **b)** secondary-irreversible (63 °C < T < 78 °C), and **c)** reversible (0 °C < T < 63 °C) crystallization regimes of L152. Positive and negative contours are shown as open and filled, respectively. Averaged 1D scattering profiles are shown on the sides.

Secondary-Irreversible Crystallization

Consistent with the pattern observed in the 1D scattering curves in the secondary-irreversible crystallization regime (Figure 4.7, solid lines), the 2D plots exhibit features characteristic of a well-defined peak shift (Figure 4.8b). The synchronous plot displays an 'angel' pattern containing two autopeaks at 0.022 and 0.048 $Å^{-1}$ that indicate the start and end of the shift. The angel pattern is analogous to the clover-leaf pattern observed in 2D analysis of WAXS but modified by intensity changes that occur concurrently with the shift resulting in asymmetry between the two autopeaks. Corresponding negative cross peaks are consistent with an overall decrease in one peak coinciding with an overall increase in the other. The asynchronous plot exhibits a butterfly pattern, consistent with a shift in peak position (rather than two stationary peaks simultaneously changing intensities in opposite directions that are also consistent with an angel pattern). The negative sign of the 'wing' below the diagonal indicates that the direction of the shift is to larger q-values.[18]

During secondary-irreversible crystallization, the average long period decreases from 28 to 13 nm. This type of peak shift can be interpreted physically as the formation of secondary lamellae within the non-crystalline regions of previously-formed lamellae, particularly in the least constrained (thickest) non-crystalline layers. This lamellar insertion explains the decrease of scattering corresponding to the largest long periods (low q) and increased scattering corresponding to long periods that are approximately half in size (higher q).

Reversible Crystallization

The synchronous 2D plot is indicative of a loss in overall intensity in a broad range of q (<0.06 $Å^{-1}$) and a mild increase at $q \sim 0.07$ $Å^{-1}$. The decrease in intensity is evident as a broad, prominent autopeak centered at 0.035 $Å^{-1}$ (Figure 4.8c). Just as the single prominent autopeak in Figure 4.7a reflected the increase of intensity as primary lamellae formed, here the autopeak reflects the loss of intensity as reversible crystallites (fringed micelles) form in the non-crystalline layers of lamellar stacks causing a decrease in the electron density contrast.[3] Weak negative cross peaks at (0.070 $Å^{-1}$, 0.035 $Å^{-1}$) indicate that as intensity decreases near 0.035 $Å^{-1}$, it simultaneously increases near 0.070 $Å^{-1}$. The corresponding autopeak (not shown) is hardly above the baseline, speaking to the small change in its intensity. The asynchronous plot again contains a single feature that is elongated along the diagonal suggesting a *mild* shift in peak position.[66] Based on the sign of the feature below the diagonal, this shift is toward larger values of q (i.e., smaller characteristic length scales).[18] Concurrently with decreasing scattering intensity that is apparent from 1D scattering curves, this slight shift in peak position is consistent with the formation of reversible crystals in the largest non-crystalline regions (corresponding to the largest L_p) first, followed by gradual growth in smaller regions. Additionally, the subtle autopeak at 0.070 $Å^{-1}$ suggests that the reversible crystals have a structural length scale of approximately 9.0 nm.

Normalization

Prior to the examination of heterospectral correlation analysis of SAXS and WAXS, this section closes with additional tools that are used when changes in both peak intensity and position are significant. In this case, 2D correlation plots, especially asyn-

chronous, can be difficult to interpret.[66] This is apparent from Figure 4.8a, in which development of intensity at the onset of crystallization, masks the shift in peak position and the expected butterfly pattern in the asynchronous plot. In addition to the change in shape of the 2D features, it has been previously reported in the context of spectroscopy that the relationship between the position of features in the 2D correlation spectra and the positions of relevant changes in the 1D spectra become less reliable as intensity changes increase.[66] To minimize effects of intensity changes, normalization of each 1D scattering curve by its overall intensity effectively re-scales all the spectra to the same intensity range, enhancing subtle features like peak shifting or broadening.

The application of Modified Mean Normalization (MMN; eqs 4.1 and 4.2)[45] has the greatest effect on the 2D correlation plots in the primary-irreversible regime (compare Figure 4.8a and Figure 4.9a). After normalization, the synchronous plot reveals an angel pattern with two autopeaks at (0.015 $Å^{-1}$, 0.015 $Å^{-1}$) and (0.037 $Å^{-1}$, 0.037 $Å^{-1}$), corresponding to long periods of 42 and 17 nm, respectively. It is of note that these values are close but not identical to the characteristic length scales obtained from the asynchronous pattern without normalization (37 and 20 nm). The latter are skewed to the intermediate values corresponding to conditions when maximum of scattering was observed (see Figure 4.9). The asynchronous plot depicts a distorted butterfly pattern that indicates a peak shift from 0.015 to 0.037 $Å^{-1}$. Hence, primary-irreversible crystallization is characterized by the steady decrease in the average long period due to the formation of crystalline structures with reduced characteristic length scales.

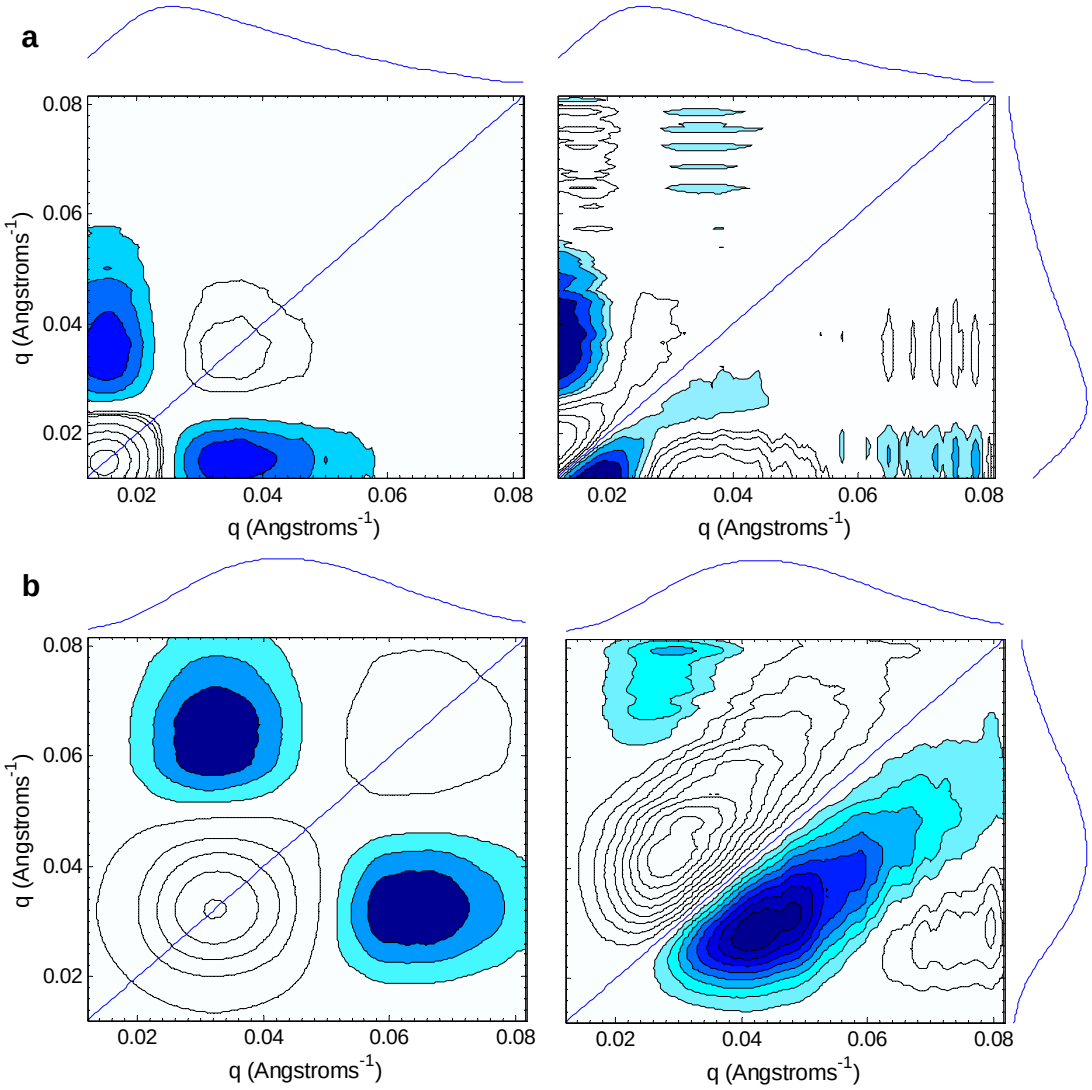

Figure 4.9 2D synchronous (left) and asynchronous (right) correlation plots computed from SAXS curves that were Lorentz-corrected and Modified Mean Normalized in **a)** primary-irreversible and **b)** reversible crystallization regimes of L152. Positive and negative contours are shown as open and filled, respectively. Averaged 1D scattering profiles are shown on the sides.

The features at high q in the asynchronous plot are the result of noise that is re-scaled by the normalization, suggesting that the application of normalization schemes requires care. Normalized 1D curves should be checked to ensure that artificial behavior is not introduced by the normalization.[48]

Since the overall intensity exhibits only weak changes in the secondary-irreversible regime, normalization has little effect here. MMN application in the reversible crystallization regime allows for the direct visualization of the previously-invisible feature at high q (compare Figure 4.9b with Figure 4.8c) indicative of structures with a characteristic length scale of approximately 9.7 nm. The angel—with autopeaks at 0.032 and 0.065 $Å^{-1}$—and distorted butterfly pattern in the synchronous and asynchronous plots, respectively, are consistent with gradual 'in-filling' of the largest non-crystalline layers. The distribution of long periods corresponding to lamellae undergoing 'in-filling' is centered at approximately 20 nm, with the smallest long periods exceeding 12 nm. The crystal in-filling, which results in an increase in the formation of structures with a reduced characteristic length-scale, is consistent with fringed micelle formation.

4.3.3 SAXS/WAXS Heterospectral Correlation Analysis

4.3.3.1 Crystallization of Random Copolymers

Heterospectral correlation analysis allows for direct examination of the coincident relationships between SAXS and WAXS in the three crystallization regimes of HPBD materials, and consequently the relationship between the development of crystals evident in WAXS and nanoscale structures (e.g., lamellae) probed by SAXS, specifically for L152.

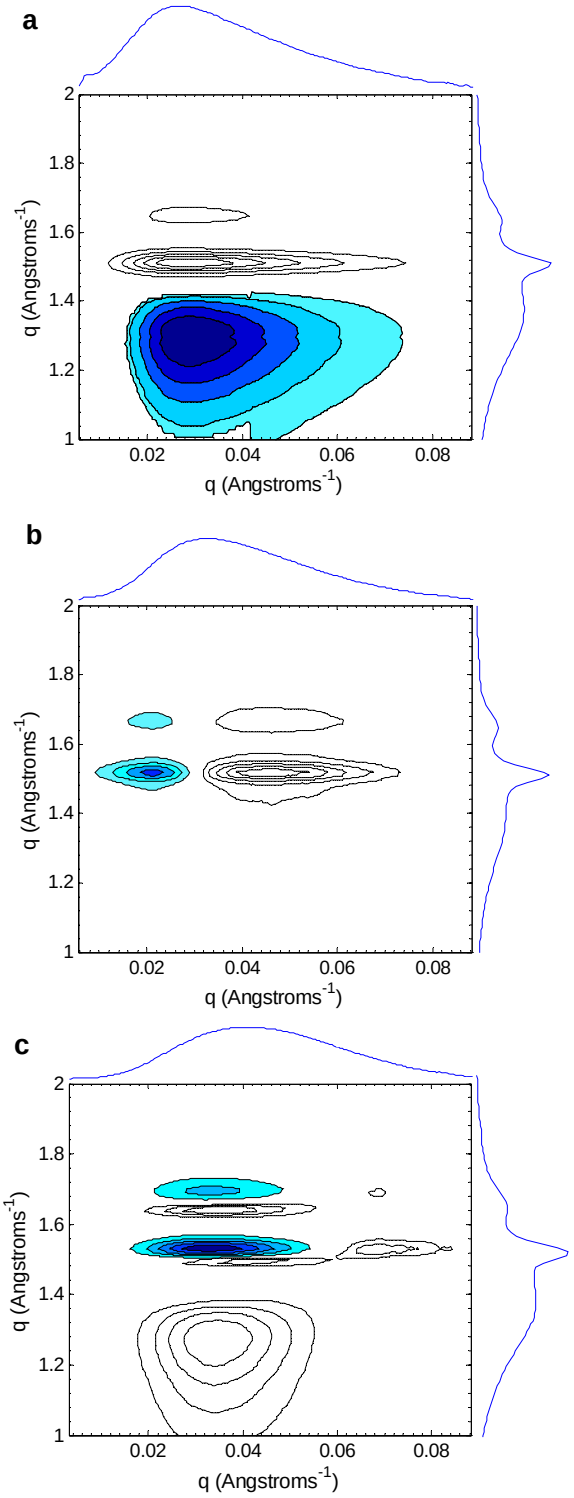

Figure 4.10 2D heterospectral correlation plots computed from Lorentz-corrected SAXS and WAXS (horizontal and vertical axes, respectively) in **a)** primary-irreversible **b)** secondary-irreversible and **c)** reversible crystallization regimes of L152. Positive and negative contours are shown as open and filled, respectively. Averaged 1D scattering profiles are shown on the sides.

Primary-Irreversible Crystallization

The strong increase in overall SAXS intensity (Figure 4.8a) and development of crystalline reflections in WAXS at the expense of the amorphous halo (Figure 4.4a) give rise to three characteristic features in the heterospectral plot for the primary-irreversible regime (Figure 4.10a); each of the WAXS features (amorphous halo and 2 crystalline reflections) is correlated with the SAXS peak that is centered at approximately 0.03 $Å^{-1}$. The crystalline reflections are positively correlated, while the amorphous halo is negatively correlated. These observations are consistent with polymer crystals organizing into lamellae with an average long period of approximately 21 nm. Hence, this heterospectral pattern, which is characteristic of rapid propagation of primary lamellae in an unconstrained melt, exhibits a change in sign of the correlation intensity along the WAXS *q*-axis (vertical direction in Figure 4.10a).

Secondary-Irreversible Crystallization

The secondary-irreversible crystallization regime is characterized by a shift in the SAXS peak at nearly constant intensity (Figure 4.8b) as well as a growth of both the WAXS crystalline reflections and the portion of the amorphous halo immediately adjacent to the (110) reflection (1.4–1.46 $Å^{-1}$ in Figure 4.4b). The shift in the SAXS peak position causes the WAXS crystalline reflections to be correlated both positively (for $q >$ 0.03 $Å^{-1}$, where SAXS intensity increases) and negatively (for $q <$ 0.03 $Å^{-1}$, where SAXS intensity decreases) with the SAXS intensity (Figure 4.10b). Changes in the amorphous halo are too weak to be observed. Negative peaks are apparent centered at (0.022 $Å^{-1}$, 1.5 $Å^{-1}$) and (0.022 $Å^{-1}$, 1.65 $Å^{-1}$) corresponding to the simultaneous increase in intensity of the crystalline reflections and the decrease of intensity in the low-*q* side of the SAXS

peak. These features indicate that crystallites form in the non-crystalline layers of the lamellar stacks having the largest long periods. Positive features centered at (0.048 $Å^{-1}$, 1.5 $Å^{-1}$) and (0.048 $Å^{-1}$, 1.65$Å^{-1}$) show that these new crystallites increase scattering corresponding to structures having a smaller long period. Hence, the development of crystallinity in the secondary-irreversible crystallization regime is attributed to secondary lamellae that form between already-formed lamellae having the largest long period essentially cutting the original long period in half. The heterospectral pattern characteristic of this physical process exhibits a change in sign of the correlation intensity along the SAXS *q*-axis (horizontal direction in Figure 4.10b).

Reversible Crystallization

Heterospectral analysis in the reversible regime reveals scattering behavior that was not immediately apparent from the conventional 2D correlation analysis of SAXS and WAXS alone. The conventional 2D SAXS correlation plots exhibited implicit evidence for the formation of crystals that have a characteristic length scale of approximately 9.0 nm, but a direct peak was not observed without normalization (Figure 4.8c). In contrast, the heterospectral plot exhibits two positive features centered at (0.068 $Å^{-1}$, 1.53 $Å^{-1}$) and (0.068 $Å^{-1}$, 1.70 $Å^{-1}$) that unambiguously correlate increases at the two crystalline reflections with SAXS scattering at large *q*.

Conventional 2D correlation analysis of WAXS in the reversible regime revealed complex behavior, including direct evidence of a shift in position of the amorphous halo and the (200) reflection coinciding with an increase in their intensities (Figure 4.4c). A shift in the (110) reflection was implied from the resolved feature at 1.46 $Å^{-1}$ (Figure 4.5). This conclusion is confirmed by the heterospectral plot, which reveals similar behavior

between the two crystalline reflections in the form of pairs of positive/negative peaks (Figure 4.10c, see negative peaks at (0.033 $Å^{-1}$, 1.53 $Å^{-1}$) and (0.033 $Å^{-1}$, 1.70 $Å^{-1}$)). These features indicate that crystallinity development in the reversible regime is marked by an increase in WAXS scattering at 1.53 and 1.70 $Å^{-1}$, which corresponds to unit cell parameters a = 7.39 Å and b = 4.94 Å, consistent with dimensions of PE crystals near room temperature.[55, 81] Simultaneously, a decrease in SAXS scattering is observed at 0.033 $Å^{-1}$, corresponding to a long period of 19 nm. This suggests that reversible crystallites preferentially form in non-crystalline layers that were too small to permit growth of secondary lamellae. The corresponding positive features are centered at (0.039 $Å^{-1}$, 1.50 $Å^{-1}$) and (0.034 $Å^{-1}$, 1.64 $Å^{-1}$) indicating that growth in crystallinity with decreasing temperature coincides with a decrease in WAXS scattering from crystals with unit cell dimensions of a = 7.66 Å and b = 5.00 Å. Although these dimensions are greater than the average expected below 60 °C,[73, 74] they can be attributed to the high-tail end of the unit cell size distribution. This heterospectral pattern, which is characteristic of fringed micelle formation in fully constrained melt, exhibits changes in sign of the correlation intensity along both the SAXS and WAXS q-axis (horizontal and vertical direction in Figure 4.10c, respectively).

No correlation was observed between SAXS intensity changes and the feature at 1.46 $Å^{-1}$ apparent in the WAXS synchronous plot in this regime. Therefore, changes in WAXS are again accounted for by variations in position and shape of only the amorphous halo and the crystalline reflections; there is no apparent need to invoke a semi-ordered phase in the spectra.

4.3.3.2 Scattering at the Onset of Crystallization

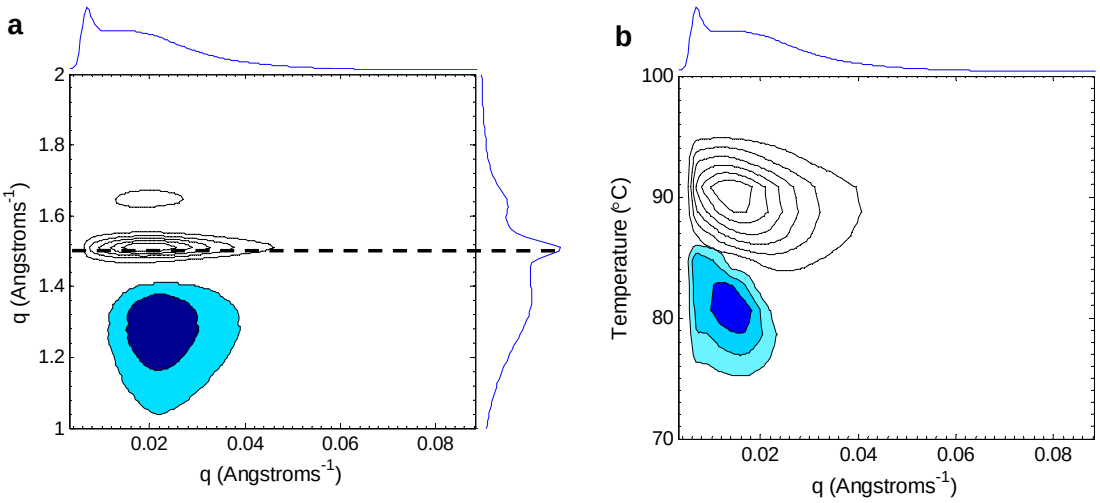

Figure 4.11 a) 2D heterospectral correlation plot computed for SAXS and WAXS curves ($I(q)$, horizontal and vertical axes, respectively) for L152 during a cooling ramp at 10 °C/min through the primary-irreversible regime. **b)** Corresponding moving window analysis on heterospectral data using a 10 °C window plotting the correlation along the (110) WAXS (dotted line in **a**) as a function of the average temperature. Positive and negative contours are shown as open and filled, respectively. Averaged 1D scattering profiles are shown on the sides in **a**.

Two-dimensional correlation analysis offers a unique approach to examine the debate about the onset of crystallization in HPBDs. Crystallization is revealed in WAXS by the appearance of the (110) and (200) reflections of the orthorhombic PE crystal. On the other hand, the appearance of a resolved peak in the SAXS curve, corresponding to a well-defined long period, occurs at lower temperatures during cooling. Instead, initial changes in SAXS scattering occur at zero scattering angle, below the beamstop. Previously, an observed lag between the increase in SAXS scattering at low q and the appearance of WAXS peaks has led some authors to invoke the interpretation of spinodal decomposition as a precursor to crystal formation.[82-85] The relationship between this initial scattering and the onset of crystallization can be examined through the application of heterospectral correlation analysis to SAXS and WAXS data.

A heterospectral correlation plot of non-Lorentz corrected SAXS and WAXS scattering curves ($I(q)$) collected during primary-irreversible crystallization (78 °C < T < 95 °C) of L152 is depicted in Figure 4.11a. This figure contains the same features as the heterospectral correlation plot for Lorentz corrected data in the same regime (Figure 4.10a): positive peaks are observed, corresponding to the primary SAXS peak and the (110) and (200) WAXS reflections and a negative peak is apparent corresponding to the primary SAXS peak and the WAXS amorphous halo. These observations are consistent with the primary-irreversible crystallization regime being dominated by the formation of orthorhombic unit cells (leading to an increase in WAXS crystalline reflections and a decrease in amorphous halo scattering) that simultaneously organize into nanoscale structures with a well-defined long period (resulting in the development of a well-defined SAXS peak).

The WAXS (110) reflection is also positively correlated with SAXS intensity at low q (<0.005 $Å^{-1}$), indicating that generally, the crystallization in the primary-irreversible regime coincides with an increase in zero angle scattering in SAXS. As stated previously, this growth occurs in the earliest stages of crystallization. As such, it may be examined by evaluating heterospectral correlation plots corresponding to small temperature windows near the start of primary-irreversible crystallization. To gauge the relationship between zero-angle scattering and crystal formation, the heterospectral correlation intensity along the WAXS (110) reflection (dashed line in Figure 4.11a) was calculated for 10 °C subsets of the SAXS/WAXS data that are shifted sequentially through high temperatures. These intensities were then used to obtain the contour plot depicting the correlation of SAXS scattering at low q with the WAXS (110) reflection as a function of

temperature in Figure 4.11b. At the earliest stages of crystallization (95 to 85 °C), the positive contour indicates that an increase in SAXS scattering at low *q*-values occurs simultaneously with growth of the (110) crystal reflection. This observation is consistent with the initial increase in SAXS intensity being due to isolated crystals in the melt, and not spinodal decomposition, in agreement with previous findings.[1, 86-89] The same conclusions were reached for all materials examined. Therefore, the dominant physical process at the early stages of crystallization of HPBD materials during cooling is the formation of isolated crystals in the melt that are engulfed by the crystalline network that propagates at lower temperatures.

4.3.4 Material Comparisons

Two-dimensional correlation analysis did not reveal differences in the evolution of morphology between the four HPBD materials examined (short linear, long linear, 3-arm star and H-polymer). All four exhibited the same characteristic length scales in the secondary-irreversible and reversible regimes. In the former, the system evolved gradually from having an average long period of 26 ± 2 nm to 13 ± 1 nm through the insertion of secondary lamellae within the greatest-spaced primary lamellae. In the following reversible regime, the system primarily lost crystal structure with a long period of 18 ± 2 nm and gained crystals with characteristic length scale of 9 ± 1 nm.

4.4 CONCLUSION

Two-dimensional correlation analysis, which is well-established in the field of vibrational spectroscopy,[17-20] proved useful in analyzing x-ray scattering data and elucidating a number of phenomena associated with quiescent crystallization of random ethylene-

copolymers. Morphology evolution in the three crystallization regimes of random copolymers—primary-irreversible, secondary-irreversible, and reversible—resulted in unique signatures in conventional 2D correlation plots of WAXS and SAXS, as well as 2D heterospectral correlation patterns, which are summarized in Table 4.2.

Table 4.2 Summary of crystallization behavior of HPBD materials.

	Crystallization Regimes		
	Primary-irreversible	**Secondary-irreversible**	**Reversible**
Morphological parameters	X_c, L_p, and Q change rapidly with hysteresis between cool and heat	X_c and L_p change slowly and Q is near maximum with hysteresis between cool and heat	X_c, L_p, and Q change rapidly with *no* hysteresis between cool and heat
SAXS	Peak intensity grows	Constant peak intensity	Peak intensity decreases
	Peak position moves to higher q		
WAXS	Decrease in intensity of amorphous halo	Change in shape and position of amorphous halo	Strong change in shape and position of amorphous halo
	Crystalline peak intensities grow, broaden, and move to higher q		
2D Hetero SAXS/WAXS	Intensity redistribution in WAXS	Intensity redistribution in SAXS	Intensity redistribution in SAXS and WAXS
Physical interpretation	Primary lamellar growth in unconstrained melt	Secondary lamellar growth in constrained melt within the largest non-crystalline regions between primary lamellae	Fringed micelle formation in severely constrained melt within largest non-crystalline layers

Two-dimensional correlation analysis SAXS was used to infer the nanoscopic superstructure development during crystallization. The morphology evolution dominating each crystallization regime resulted in 2D correlation features that are associated with primary lamellar propagation, secondary lamellar insertion, and fringed micelle 'infilling.' Additionally, it was demonstrated that when structure evolution is dominated by

strong intensity changes, further insight may be gained by minimizing this effect through normalization schemes.

Heterospectral analysis provided insight about the direct relationship between unit cell growth (as given by WAXS) and simultaneous their organization into superstructures (as given by SAXS). Each crystallization regime exhibited unique 2D heterospectral patterns emphasizing the different physics that govern crystallization in the three crystallization regimes of random copolymers. Propagation of primary lamellae through an unconstrained melt during primary-irreversible crystallization is characterized by correlation features that are negative at low WAXS wavevectors and positive at high WAXS wavevectors (Figure 4.10a). Growth of secondary lamellae within the largest non-crystalline layers between primary lamellae during secondary-irreversible crystallization is characterized by correlation features that are negative and positive at low and high SAXS wavevectors, respectively. Fringed-micelle formation in severely constrained non-crystalline regions is characterized by changes in sign of the correlation intensity along both the SAXS and WAXS wavevectors. These heterospectral patterns can be used to fingerprint the corresponding physical processes in other polymer systems.

Additionally, heterospectral analysis corresponding to the onset of crystallization revealed that the initial increase in scattering at low q during cooling is the result of isolated lamellae in the melt, and not spinodal decomposition, consistent with conclusions from previous studies.[1, 86-89]

WAXS data in the three crystallization regimes of random copolymers revealed no evidence for the formation of a semi-ordered phase that has been proposed in previous studies.[5, 7, 34, 35, 37] Those features that could be attributed to the reflections of a crystal-

like semi-ordered phase, lead to inconsistent behavior of this supposed 'phase.' We offer an alternative explanation in which these features are ascribed to thermal contraction of the crystalline phase, loss of coherent unit cell growth at low temperatures, and a change in shape and position of the amorphous halo. The latter observation is explained by thermal contraction of the non-crystalline material and its enrichment with butyl branches nearest to the crystal surface that are excluded as crystallization proceeds. The rejection of chain defects also causes increased crowding at the crystal interface resulting in heterogeneity in the non-crystalline phase. This heterogeneity is evident at lower temperatures associated with the formation of secondary lamellae and fringed micelles in a constrained melt. Further insight into the development of this heterogeneity can be achieved through the examination of materials with varying SCB content. One would expect that the amount of non-crystalline heterogeneity would increase with crystal defects.[37, 57] Hence, the application of 2D correlation analysis may provide further insight into this phenomenon if applied to highly-branched systems.

Two-dimensional correlation analysis of WAXS data proved to be highly sensitive to spectral changes, revealing, for example, subtle, yet complex behavior associated with fringed micelle formation and very mild shifting of the crystalline reflections due to thermal contraction. This sensitivity of 2D correlation analysis makes it a powerful tool to study materials with different crystal morphs that are difficult to resolve from 1D curves, such as may be the case with some block copolymers.[90]

4.5 ACKNOWLEDGEMENTS

This work would not have been possible without ExxonMobil Research and Engineering Company (Clinton, NJ), particularly Dr. David Lohse and his team, who provided materials and financial support. We must thank the beamline staff at beamline X27C at NSLS BNL (Dr. Lixia Rong and Jie Zhu) and beamline 7.3.3 at ALS LBL (Dr. Alexander Hexemer and Eliot Gann). X-ray data was collected with the assistance of Zuleikha Kurji (Caltech). Part of this work was also funded by the National Science Foundation (DMR-0505393 and GOALI-0523083). Manuscript preparation was assisted by Prof. Julia Kornfield (Caltech).

4.6 REFERENCES

1. Akpalu, Y. A.; Amis, E. J., Evolution of density fluctuations to lamellar crystals in linear polyethylene. *Journal of Chemical Physics* **1999,** 111, (18), 8686-8695.
2. Goderis, B.; Peeters, M.; Mathot, V. B. F.; Koch, M. H. J.; Bras, W.; Ryan, A. J.; Reynaers, H., Morphology of homogeneous copolymers of ethylene and 1-octene. III. Structural changes during heating as revealed by time-resolved SAXS and WAXD. *Journal of Polymer Science Part B-Polymer Physics* **2000,** 38, (15), 1975-1991.
3. Mathot, V. B. F.; Scherrenberg, R. L.; Pijpers, M. F. J.; Bras, W., Dynamic DSC, SAXS and WAXS on homogeneous ethylene-propylene and ethylene-octene co-polymers with high comonomer contents. *Journal of Thermal Analysis* **1996,** 46, (3-4), 681-718.
4. McFaddin, D. C.; Russell, K. E.; Wu, G.; Heyding, R. D., Characterization of Poly-ethylenes by X-Ray-Diffraction and C-13-Nmr - Temperature Studies and the Nature of the Amorphous Halo. *Journal of Polymer Science Part B-Polymer Physics* **1993,** 31, (2), 175-183.
5. Sajkiewicz, P.; Hashimoto, T.; Saijo, K.; Gradys, A., 'Intermediate phase' in poly(ethylene) as elucidated by the WAXS. Analysis of crystallization kinetics. *Polymer* **2005,** 46, (2), 513-521.
6. Strobl, G. R.; Schneider, M. J.; Voigtmartin, I. G., Model of Partial Crystallization and Melting Derived from Small-Angle X-Ray-Scattering and Electron-Microscopic Studies on Low-Density Polyethylene. *Journal of Polymer Science Part B-Polymer Physics* **1980,** 18, (6), 1361-1381.

7. Russell, K. E.; Hunter, B. K.; Heyding, R. D., Polyethylenes Revisited - Waxs and the Phase-Structure. *European Polymer Journal* **1993,** 29, (2-3), 211-217.

8. Rabiej, S.; Goderis, B.; Janicki, J.; Mathot, V. B. F.; Koch, M.; Reynaers, H.; Wlochowicz, A. In *Influence of thermal treatment on the supermolecular structure of homoueneous polyethylene-1-octene copolymers*, 2003; Inst Chemical Fibres: 2003; pp 28-31.

9. Fernandez-Ballester, L.; Gough, T.; Meneau, F.; Bras, W.; Ania, F.; Balta-Calleja, F. J.; Kornfield, J. A., Simultaneous birefringence, small- and wide-angle X-ray scattering to detect precursors and characterize morphology development during flow-induced crystallization of polymers. *Journal of Synchrotron Radiation* **2008,** 15, (2), 185-190.

10. Vanden Eynde, S.; Mathot, V.; Koch, M. H. J.; Reynaers, H., Thermal behaviour and morphology of homogeneous ethylene-propylene and ethylene-1-butene copolymers with high comonomer contents. *Polymer* **2000,** 41, (9), 3437-3453.

11. Wang, Z.; Wang, H.; Shimizu, K.; Dong, K.-Y.; Hsiao, B. S.; Han, C. C., Structural and morphological development in poly(ethylene-co-hexene) and poly(ethylene-co-butylene) blends due to the competition between liquid-liquid phase separation and crystallization. *Polymer* **2005,** 46, 2675-2684.

12. Nogales, A.; Hsiao, B. S.; Somani, R. H.; Srinivas, S.; Tsou, A. H.; Balta-Calleja, F. J.; Ezquerra, T. A., Shear-induced crystallization of isotactic polypropylene with different molecular weight distributions: in situ small- and wide-angle X-ray scattering studies. *Polymer* **2001,** 42, (12), 5247-5256.

13. Liang, S.; Wang, K.; Tang, C. Y.; Zhang, Q.; Du, R. N.; Fua, Q., Unexpected molecular weight dependence of shish-kebab structure in the oriented linear low density polyethylene/high density polyethylene blends. *Journal of Chemical Physics* **2008,** 128, (17), 9.

14. Peeters, M.; Goderis, B.; Reynaers, H.; Mathot, V., Morphology of Homogeneous Copolymers of Ethylene and 1-Octene. II. Structural Changes on Annealilng. *Journal of Polymer Science: Part B: Polymer Physics* **1999,** 37, (1), 83-100.

15. Heeley, E. L.; Gough, T.; Bras, W.; Gleeson, A. J.; Coates, P. D.; Ryan, A. J., Polymer processing: Using synchrotron radiation to follow structure development in commercial and novel polymer materials. *Nuclear Instruments & Methods in Physics Research Section B - Beam interactions with materials and atoms* **2005,** 238, (1-4), 21-27.

16. Struik, L. C. E., The Mechanical and Physical Aging of Semicrystalline Polymers .1. *Polymer* **1987,** 28, (9), 1521-1533.

17. Noda, I. In *Recent advancement in the field of two-dimensional correlation spectroscopy*, 2008; Elsevier Science Bv: 2008; pp 2-26.

18. Noda, I.; Ozaki, Y., *Two-Dimensional Correlation Spectroscopy*. John Wiley & Sons Ltd.: West Sussex 2004.

19. Noda, I., Generalized Two-Dimensional Correlation Method Applicable to Infrared, Raman, and Other Types of Spectroscopy. *Applied Spectroscopy* **1993,** 47, (9), 1329-1336.

20. Noda, I., Determination of Two-Dimensional Correlation Spectra Using the Hilbert Transform. *Applied Spectroscopy* **2000,** 54, (7), 994-999.

21. Ashton, L.; Boguslawa, C. M. B.; Blanch, E. W. In *Application of two-dimensional correlation analysis to Raman optical activity*, 2006; Elsevier Science Bv: 2006; pp 61-71.

22. Goormaghtigh, E.; Ruysschaert, J. M.; Raussens, V., Evaluation of the information content in infrared spectra for protein secondary structure determination. *Biophysical Journal* **2006,** 90, (8), 2946-2957.

23. Murayama, K.; Czarnik-Matusewicz, B.; Wu, Y.; Tsenkova, R.; Ozaki, Y., Comparison between Conventional Spectral Analysis Methods, Chemometrics, and Two-Dimensional Correlation Spectroscopy in the Analysis of Near-Infrared Spectra of Protein. *Applied Spectroscopy* **2000,** 54, (7), 978-985.

24. Huang, J. Y.; Shih, W. T. In *Probing field-induced submolecular motions in a ferroelectric liquid crystal mixture with time-resolved two-dimensional infrared spectroscopy*, 2006; Iop Publishing Ltd: 2006; pp 7593-7603.

25. Thomas, M.; Richardson, H. H., Two-dimensional FT-IR correlation analysis of the phase transitions in a liquid crystal, 4 '-n-octyl-4-cyanobiphenyl (8CB). *Vibrational Spectroscopy* **2000,** 24, (1), 137-146.

26. Watanabe, S.; Noda, I.; Ozaki, Y., Thermally induced conformational and structural disordering in polyethylene crystal studied by near-infrared spectroscopy. *Polymer* **2008,** 49, (3), 774-784.

27. Gregoriou, V. G.; Noda, I.; Dowrey, A. E.; Marcott, C.; Chao, J. L.; Palmer, R. A., Dynamic Rheooptical Characterization of a Low-Density Polyethylene Perdeuterated High-Density Polyethylene Blend by 2-Dimensional Step-Scan Ftir Spectroscopy. *Journal of Polymer Science Part B-Polymer Physics* **1993,** 31, (12), 1769-1777.

28. Jung, Y. M.; Shin, H. S.; Kim, S. B.; Noda, I., Two-dimensional gradient mapping technique useful for detailed spectral analysis of polymer transition temperatures. *Journal of Physical Chemistry B* **2008,** 112, (12), 3611-3616.

29. Sasic, S.; Zhang, J. M.; Ozaki, Y., Detailed interpretation of the results of two-dimensional correlation analysis of infrared spectra obtained during isothermal crystallization of isotactic polystyrene and poly(3-hydroxybutyrate). *Vibrational Spectroscopy* **2007,** 44, (1), 50-55.

30. Zhang, J. M.; Duan, Y. X.; Sato, H.; Men, D. Y.; Yan, S. K.; Noda, I.; Ozaki, Y., Initial crystallization mechanism of isotactic polystyrene from different states. *Journal of Physical Chemistry B* **2005,** 109, (12), 5586-5591.

31. Kim, H. J.; Bin Kim, S.; Kim, J. K.; Jung, Y. M., Two-dimensional heterospectral correlation analysis of wide-angle X-ray scattering and infrared spectroscopy for specific chemical interactions in weakly interacting block copolymers. *Journal of Physical Chemistry B* **2006,** 110, (46), 23123-23129.

32. Noda, I. Dynamic Infrared Dichroism and Two-Dimensional Correlation Spectroscopy. Univeristy of Tokyo, 1997.

33. Simanke, A. G.; Alamo, R. G.; Galland, G. B.; Mauler, R. S., Wide-angle X-ray scattering of random metallocene-ethylene copolymers with different types and concentration of comonomer. *Macromolecules* **2001,** 34, (20), 6959-6971.

34. Baker, A. M. E.; Windle, A. H., Evidence for a partially ordered component in polyethylene from wide-angle X-ray diffraction. *Polymer* **2001,** 42, (2), 667-680.

35. Rabiej, S.; Bnias, W.; Binias, D., The Transition Phase in Polyethylenes - WAXS and Raman Investigations. *Fibres & Textiles in Eastern Europe* **2008,** 16, (6), 57-62.

36. Rabiej, S. In *WAXS investigations of the amorphous phase structure in linear polyethylene and ethylene-1-octene homogeneous copolymers*, 2005; Inst Chemical Fibres: 2005; pp 30-34.

37. Monar, K.; Habenschuss, A. In *Modeling the principal amorphous halo in quiescent melts of polyethylene and ethylene copolymers using wide-angle X-ray scattering and its implications*, 1999; John Wiley & Sons Inc: 1999; pp 3401-3410.

38. Androsch, R.; Blackwell, J.; Chvalun, S. N.; Wunderlich, B., Wide- and small-angle X-ray analysis of poly(ethylene-co-octene). *Macromolecules* **1999,** 32, (11), 3735-3740.

39. Kolesov, I. S.; Androsch, R.; Radusch, H. J. In *Non-isothermal crystallization of polyethylenes as function of cooling rate and concentration of short chain branches*, 2004; Kluwer Academic Publ: 2004; pp 885-895.

40. Androsch, R.; Wunderlich, B., Analysis of the degree of reversibility of crystallization and melting in poly(ethylene-co-1-octene). *Macromolecules* **2000,** 33, (24), 9076-9089.

41. Hu, W. G.; Srinivas, S.; Sirota, E. B., Crystalline structure and properties of EP and EB copolymers by solid-state NMR, DSC, and WAXS. *Macromolecules* **2002,** 35, (13), 5013-5024.

42. Azzurri, F.; Gomez, M. A.; Alfonso, G. C.; Ellis, G.; Marco, C. In *Time-resolved SAXS/WAXS studies of the polymorphic transformation of 1-butene/ethylene copolymers*, 2004; Marcel Dekker Inc: 2004; pp 177-189.

43. Goderis, B.; Reynaers, H.; Koch, M. J., Primary and Secondary Crystallization in a Homogeneous Ethylene-1-Octene Copolymer: Crystallinity Heterogeneity Studied by SAXS. *Macromolecules* **2002,** 25, 5840-5853.

44. Cser, F., About the Lorentz correction used in the interpretation of small angle X-ray scattering data of semicrystalline polymers. *Journal of Applied Polymer Science* **2001,** 80, (12), 2300-2308.

45. Wang, Y. W.; Gao, W. Y.; Noda, I.; Yu, Z. W. In *A modified mean normalization method to reduce the effect of peak overlap in two-dimensional correlation spectroscopy*, 2006; Elsevier Science Bv: 2006; pp 128-133.

46. Noda, I.; Ozaki, Y., Response to "some comments on tine application of two-dimensional correlation spectroscopy and normalization of the dynamic spectra" by Miroslaw A. Czarnecki. *Applied Spectroscopy* **2003,** 57, (1), 110-112.

47. Czarnecki, M. A., Some comments on the application of two-dimensional correlation spectroscopy and normalization of the dynamic spectra. *Applied Spectroscopy* **2003,** 57, (1), 107-109.

48. Diewok, J.; Ayora-Canada, M. J.; Lendl, B., 2D correlation spectroscopy and multivariate curve resolution in analyzing pH-dependent evolving systems monitored by FT-IR spectroscopy, a comparative study. *Analytical Chemistry* **2002,** 74, (19), 4944-4954.

49. Morita, S.; Shinzawa, H.; Tsenkova, R.; Noda, I.; Ozaki, Y. In *Computational simulations and a practical application of moving-window two-dimensional correlation spectroscopy*, 2006; Elsevier Science Bv: 2006; pp 111-120.

50. Shinzawa, H.; Morita, S.; Noda, I.; Ozaki, Y. In *Effect of the window size in moving-window two-dimensional correlation analysis*, 2006; Elsevier Science Bv: 2006; pp 28-33.

51. Alizadeh, A.; Richardson, L.; Xu, J.; McCartney, S.; Marand, H.; Cheung, Y. W.; Chum, S., Influence of Structural and Topological Constraints on the Crystallization and Melting Behavior of Polymers. 1. Ethylene/1-Octene Copolymers. *Macromolecues* **1999,** 32, 6221-6235.

52. Rabiej, S.; Goderis, B.; Janicki, J.; Mathot, V. B. F.; Koch, M. H. J.; Groeninckx, G.; Reynaers, H.; Gelan, J.; Wlochowicz, A., Characterization of the dual crystal population in an isothermally crystallized homogeneous ethylene-1-octene copolymer. *Polymer* **2004,** 45, 8761-8778.

53. Androsch, R.; Wunderlich, B., Specific reversible melting of polyethylene. *Journal of Polymer Science Part B-Polymer Physics* **2003,** 41, (18), 2157-2173.

54. Nam, J. Y.; Kadomatsu, S.; Saito, H.; Inoue, T., Thermal reversibility in crystalline morphology of LLDPE crystallites. *Polymer* **2002,** 43, (7), 2101-2107.

55. Swan, P. R., Polyethylene Unit Cell Variations with Temperature. *Journal of Polymer Science* **1962,** 56, (164), 403-&.

56. Basiura, M.; Gearba, R. I.; Ivanov, D. A.; Janicki, J.; Reynaers, H.; Groeninckx, G.; Bras, W.; Goderis, B., Rapidly cooled polyethylenes: On the thermal stability of the semicrystalline morphology. *Macromolecules* **2006,** 39, (24), 8399-8411.

57. Alamo, R.; Domszy, R.; Mandelkern, L., Thermodynamic and Structural-Properties of Copolymers of Ethylene. *Journal of Physical Chemistry* **1984,** 88, (26), 6587-6595.

58. Shirayama, K.; Watabe, H.; Kita, S., Effects of Branching on Some Properties of Ethylene Alpha-Olefin Copolymers. *Makromolekulare Chemie* **1972,** 151, (JAN20), 97-&.

59. Swan, P. R., Polyethylene Unit Cell Variations with Branching. *Journal of Polymer Science* **1962,** 56, (164), 409-&.

60. Perez, E.; Benavente, R.; Quijada, R.; Narvaez, A.; Galland, G. B., Structure characterization of copolymers of ethylene and 1-octadecene. *Journal of Polymer Science Part B-Polymer Physics* **2000,** 38, (11), 1440-1448.

61. Peeters, M.; Goderis, B.; Vonk, C.; Reynaers, H.; Mathot, V., Morphology of Homogeneous Copolymers of Ethene and 1-Octene. I. Influence of Thermal History on Morphology. *Journal of Polymer Science: Part B: Polymer Physics* **1997,** 35, 2689-2713.

62. Howard, P. R.; Crist, B., Unit-Cell Dimensions in Model Ethylene Butene-1 Copolymers. *Journal of Polymer Science Part B-Polymer Physics* **1989,** 27, (11), 2269-2282.

63. Qiu, J.; Xu, D.; Zhao, J.; Niu, Y.; Wang, Z., New Insights into the Multiple Melting Behaviors of the Semicrystalline Ethylene-Hexene Copolymer: Origins of Quintuple Melting Peaks. *Journal of Polymer Science: Part B: Polymer Physics* **2008,** 46, 2100-2115.

64. Quinn, F. A.; Mandelkern, L., Thermodynamics of Crystallization in High Polymers - Poly-(Ethylene). *Journal of the American Chemical Society* **1958,** 80, (13), 3178-3182.

65. Bunn, C. W., The crystal structure of long-chain normal paraffin hydrocarbons. The "shape" of the > CH2 group. *Transactions of the Faraday Society* **1939,** 35, (1), 0482-0490.

66. Czarnecki, M. A., Interpretation of two-dimensional correlation spectra: Science or art? *Applied Spectroscopy* **1998,** 52, (12), 1583-1590.

67. Morita, S.; Miura, Y. F.; Sugi, M.; Ozaki, Y., New correlation indices invariant to band shifts in generalized two-dimensional correlation infrared spectroscopy. *Chemical Physics Letters* **2005,** 402, (1-3), 251-257.

68. Noda, I., 2-Dimensional Infrared (2d Ir) Spectroscopy - Theory and Applications. *Applied Spectroscopy* **1990,** 44, (4), 550-561.

69. Gericke, A.; Gadaleta, S. J.; Brauner, J. W.; Mendelsohn, R., Characterization of biological samples by two-dimensional infrared spectroscopy: Simulation of frequency, bandwidth, and intensity changes. *Biospectroscopy* **1996,** 2, (6), 341-351.

70. Nabet, A.; Auger, M.; Pezolet, M., Investigation of the temperature behavior of the bands due to the methylene stretching vibrations of phospholipid acyl chains by two-dimensional infrared correlation spectroscopy. *Applied Spectroscopy* **2000,** 54, (7), 948-955.

71. Davis, G. T.; Eby, R. K.; Colson, J. P., Thermal Expansion of Polyethylene Unit Cell-Effect of Crystal Size. *Bulletin of the American Physical Society* **1970,** 15, (3), 330-&.

72. Davis, G. T.; Eby, R. K.; Colson, J. P., Thermal Expansion of Polyethylene Unit Cell - Effect of Lamella Thickness. *Journal of Applied Physics* **1970,** 41, (11), 4316-&.

73. Watanabe, S.; Sano, N.; Noda, I.; Ozaki, Y., Surface Melting and Lamella Rearrangement Process in Linear Low Density Polyethylene. *Journal of Physical Chemistry B* **2009,** 113, (11), 3385-3394.

74. Knudsen, K. D.; Hemmingsen, P. V.; We, F., Temperature-induced structural changes in some random ethylene/1-hexene copolymers. *Polymer* **2007,** 48, (11), 3148-3161.

75. Sasic, S.; Muszynski, A.; Ozaki, Y., A new possibility of the generalized two-dimensional correlation spectroscopy. 1. Sample-sample correlation spectroscopy. *Journal of Physical Chemistry A* **2000,** 104, (27), 6380-6387.

76. Sasic, S.; Ozaki, Y., Comparison of principal component analysis and generalized two-dimensional correlation spectroscopy: Spectral analysis of synthetic model system and near-infrared spectra of milk. *Applied Spectroscopy* **2001,** 55, (1), 29-38.

77. Wang, Y. W.; Gao, W. Y.; Wang, X. G.; Yu, Z. W. In *A novel normalization method based on principal component analysis to reduce the effect of peak overlaps in two-dimensional correlation spectroscopy*, 2008; Elsevier Science Bv: 2008; pp 66-72.

78. Li, Y.; Akpalu, Y. A., Probing the Melting Behavior of a Homogeneous Ethylene/1-Hexene Copolymer by Small-Angle Light Scattering. *Macromolecules* **2004,** 27, 7265-7277.

79. Schouterden, P.; Vandermarliere, M.; Riekel, C.; Koch, M. H. J.; Groeninckx, G.; Reynaers, H., Characterization of the Morphological-Changes in Linear Low-Density Polyethylene During the Melting Process Using Synchrotron Radiation. *Macromolecules* **1989,** 22, (1), 237-244.

80. Vonk, C. G.; Koga, Y., An X-Ray-Diffraction Study of Nonlinear Polyethylene .2. Small-Angle Scattering Observations near the Melting-Point. *Journal of Polymer Science Part B-Polymer Physics* **1985,** 23, (12), 2539-2548.

81. Wiley Database of Polymer Properties. In John Wiley & Sons, Inc.: 1999-2009.

82. Cahn, J. W.; Hilliard, J. E., Free Energy of a Nonuniform System .1. Interfacial Free Energy. *Journal of Chemical Physics* **1958,** 28, (2), 258-267.

83. Cahn, J. W., Phase Separation by Spinodal Decomposition in Isotropic Systems. *Journal of Chemical Physics* **1965,** 42, (1), 93-&.

84. Cook, H. E., Brownian Motion in Spinodal Decomposition. *Acta Metallurgica* **1970,** 18, (3), 297-&.

85. Stribeck, N.; Nochel, U.; Funari, S. S., Melting and Crystallization of Differently Oriented Sets of Crystallites in Hard-Elastic Polypropylene. *Macromolecules* **2009,** 42, (6), 2093-2101.

86. Panine, P.; Urban, V.; Boesecke, P.; Narayanan, T. In *Combined small- and wide-angle X-ray scattering study of early stages of polymer crystallization*, 2003; Blackwell Munksgaard: 2003; pp 991-994.

87. Akpalu, Y.; Kielhorn, L.; Hsiao, B. S.; Stein, R. S.; Russell, T. P.; Egmond, J. v.; Muthukumar, M., Structure Development during Crystallization of Homogeneous Copolymers of Ethene and 1-Octene: Time-Resolved Synchrotron X-ray and SALS Measurements. *Macromolecules* **1999,** 32, 765-770.

88. Wang, H., SANS study of the early stages of crystallization in polyethylene solutions. *Polymer* **2006,** 47, (14), 4897-4900.

89. Panine, P.; Di Cola, E.; Sztucki, M.; Narayanan, T., Early stages of polymer melt crystallization. *Polymer* **2008,** 49, (3), 676-680.

90. Hamley, I. W.; Parras, P.; Castelletto, V.; Castillo, R. V.; Muller, A. J.; Pollet, E.; Dubois, P.; Martin, C. M., Melt structure and its transformation by sequential crystallization of the two blocks within poly(L-lactide)-block-poly(epsilon-caprolactone) double crystalline diblock copolymers. *Macromolecular Chemistry and Physics* **2006,** 207, (11), 941-953.